Fully distributed cooperation for networked uncertain mobile manipulators

Yi Ren, Stefan Sosnowski, Sandra Hirche, *Fellow, IEEE*

***Abstract*—This paper investigates a fully distributed cooperation scheme for networked mobile manipulators. To achieve cooperative task allocation in a distributed way, an adaptation-based estimation law is established for each robotic agent to estimate the desired local trajectory. In addition, wrench synthesis is analyzed in detail to lay a solid foundation for tight cooperation tasks. Together with the estimated task, a set of distributed adaptive controllers is proposed to achieve motion synchronization of the mobile manipulator ensemble over a directed graph with a spanning tree irrespective of the kinematic and dynamic uncertainties in both the mobile manipulators and the tightly grasped object. The controlled synchronization alleviates the performance degradation caused by the estimation/tracking discrepancy during the transient phase. The proposed scheme requires no persistent excitation condition and avoids the use of noisy Cartesian-space velocities. Furthermore, it is independent from the object's center of mass by employing formation-based task allocation and a task-oriented strategy. These attractive attributes facilitate the practical application of the scheme. It is theoretically proven that convergence of the cooperative task tracking error is guaranteed. Simulation results, as well as manipulation experiments with three mobile manipulators involved, validate the efficacy and demonstrate the expected performance of the proposed scheme.**

***Index Terms*—Distributed cooperation, networked mobile manipulators, uncertain kinematics and dynamics, adaptive control, cooperative task allocation**

I. Introduction

MOBILE manipulators, which combine the manipulation dexterity of robotic arms and the maneuverability of mobile platforms, tend to be far more versatile than the conventional base-fixed counterparts due to their enlarged workspace and the potential for wider application scenarios, e.g., part transfer, rescue and remote maintenance in outdoor environment, etc. [1]. Therefore, the multiple mobile manipulator ensemble has drawn increasing attention of the research community in recent years owing to its ability to perform more complex tasks such as transporting or assembling large and heavy objects that cannot be achieved by a single mobile robot. These attractive advantages come at the cost of a major increase in complexity for modelling and controlling such systems, especially for the case considered in this paper that a team of uncertain mobile manipulators cooperate to grasp and manipulate an unknown object. Introduction of the mobile platform, typically a nonholonomic vehicle, not only creates a high degree of redundancy but also imposes nonintegrable constraints on the kinematics, which hinders direct control of the whole system and restricts its instantaneous motion capability. In addition, interactions between the mobile platform and the manipulator necessitate the integrated modelling method of both the system dynamics and kinematics. Furthermore, the tightly grasped object and the mobile manipulator ensemble form connected kinematics with a star topology, which leads to the imposition of a set of kinematic/dynamic constraints on each mobile manipulator and the degradation of the degrees of freedom. This will be accompanied by the generation of internal forces that require regulation. Ignoring the control of these internal forces may result in grasp failure or unrecoverable damage to the end-effector (EE) or the object.

The core problem in multi-robot manipulation besides the modelling complexity mentioned above lies in the establishment of a fully distributed scheme for the inherently centralized cooperation task, especially under certain communication constraint and ubiquitous model uncertainties. Note that the scheme presented in this paper may easily be extended to other cases by relaxing some of the considered constraints.

A. Related Work

Cooperation and coordination of multi-agent system have been well recognized as an important technique to enhance flexibility and improve efficiency [2]. The endeavor to achieve manipulation and transportation of an object by a multi-arm system in a cooperative manner generally comprises three control schemes: centralized control [3], decentralized control [4], [5] and distributed control [6], [7]. Under the centralized architecture, a global coordinator either in a leader robot or in another host computer facilitates object-oriented control with the help of available global states of the robotic system. Force/position control [8] and impedance control [9], [10] are both extensively utilized to achieve safe interaction between the dual-arm manipulators and the grasped object. Extension of this cooperative manner to multiple mobile manipulators [11] and its model-based control can benefit from the comprehensive interaction dynamic model from the perspective of kinematic constraint [12]. Although the centralized architecture shows sufficient power to control multi-robot system and can easily incorporate the single-robot control strategy, assumption of the existence of a central station makes the

The authors are with the Chair of Information-oriented Control, Department of Electrical and Computer Engineering, Technische Universität München, Munich, Germany. (yi.ren@tum.de; sosnowski@tum.de; hirche@tum.de).

This work was supported by the Joint Sino-German Research Project "Control and optimization for event-triggered networked autonomous multi-agent systems (COVEMAS)", which is funded through the German Research Foundation (DFG) and the National Natural Science Foundation of China (NSFC).

This paper has supplementary downloadable material available at http://ieeexplore.ieee.org.

whole system more vulnerable and its malfunction will lead to the breakdown of the whole system [13]. The decentralized scheme requires no explicit communication, but either assumes that all the robots know the cooperative task in advance or uses intention estimation in the case that no uncertainties exist. On the contrary, as a more promising and preferable alternative, the distributed approach predominates when robot collectives are subjected to some inevitable communication constraints and high manipulation performance is still a high priority. Specifically, it is unreasonable to assume there exists a coordinator for the case studied here since all team members are mobile.

To achieve distributed control of a multi-arm system, a leader-follower approach is an option generally associated with the schemes that are devoted to reducing the communication burden while trying to achieve as much as possible. Based on the diagram of impedance dynamics and leader-follower scheme, coordinated motion control for multiple mobile manipulators is employed to achieve cooperative object manipulation [14]. Inspired by a team of people moving a table, the followers can implement an impedance law similar to the leader's either by estimating the leader's desired motion [5] or by taking the contact force as the leader's motion intention [15]. This innovation enables the whole system to work under implicit communication. Another interesting work [16] that does not require communication achieves force coordination between leader and follower only by measuring the object's motion as the feedback. However, the assumptions that all followers act passively in the transport task in [5], [14], that desired velocity of the grasped object is constant and available to each agent in [15], that the attachment points of the collectives are centrosymmetric around the center of mass (COM) of the object in [16], act as the primary factors that impede the applications of their works to our case.

The idea that successful object transportation and manipulation is generally strongly related to the robot formation has also been continuously inspiring related works [17], [18]. Along with the rapid advances in graph theory and control philosophy of multi-agent systems, the distributed scheme under explicit communication plays an important role in the formation control of multiple mobile robots [19], [20]. The challenge existing in formation-based transport task for a multiple mobile manipulator ensemble lies in the design of a distributed control law to achieve a global behavior in cooperative manner with limited local information and constrained communication [21]. A typical schema [22] employs a set of distributed controller/observer to achieve relative formation of the multi-arm system. Convergent estimation of the collective states by a local observer bridges the gap between the local control and the global cooperative behavior, thus a distributed cooperation is achieved [23].

To further maintain high performance when the mobile robot team executes tightly cooperative tasks whilst suffering from the inevitable uncertainties of the robot dynamics, an adaptive mechanism is introduced into the architecture, based on either impedance control [24] or force/position control [22]. More complicate cases in which the dynamic uncertainty and communication constraints (e.g., the jointly connected communication topology [2]) coexist can be easily tackled by embedding the parameter adaptation into the respective control scheme. Recent representative work [25] employs robust adaptive control to concurrently address dynamic uncertainties and external disturbances. The dependence on the communication network and costly force/torque sensors is further eliminated by introducing the assumption that all the robot agents know the desired trajectory and exact grasp parameters in advance. In addition, to cope with uncertainties of the grasped object, a distributed approach is presented in [26] to estimate the object's dynamic/kinematic parameters by moving the object with specific applied forces. Based on this estimation process, the cooperative manipulation of an unknown object can be further expected at the expense of a small bounded tracking error by a two-stage decentralized scheme [27], [28]. While these works either assume that the object's COM is known to all robotic agents or employ a separate step to estimate the object's COM, the prerequisite persistent excitation condition may restrict their range of practical application.

In addition, the robotic collectives in the above-mentioned works are free of kinematic uncertainties. However, the uncertain grasp points on the object, the indeterminate end-effector configuration, the unavoidable machining error and the assembly error all result in kinematic uncertainties. A cooperative transport task is very sensitive to kinematic uncertainties of the interconnected system. Since the manipulators rigidly contact with the object, a small kinematic discrepancy may lead to a large tracking error and build-up of the internal force. Adaptability to kinematic uncertainties endows the multiple robotic system with improved intelligence and flexibility. All of these demonstrate the necessity of handling the kinematic uncertainties with care.

B. Contribution

Multi-arm manipulation is associated with tight cooperation in which both dynamic and kinematic constraints are applied to each of the mobile manipulators. In addition, the cooperative task should be well allocated among the robotic agents in a distributed way. In light of the above discussions, this study contributes a fully distributed control scheme for a team of networked mobile manipulators to cooperatively manipulate an unknown object with the following advantages which distinguish our proposed scheme from existing approaches:

1) Uncertain dynamics/interconnected kinematics and limited communication are addressed comprehensively based on adaptive control.
2) Task allocation and cooperative control are fully distributed. The synchronization idea is fulfilled through the design of the whole control scheme, which can alleviate the performance degradation caused by the estimation and tracking discrepancy during the transient phase.
3) No persistent excitation condition is required and the use of noisy Cartesian-space velocities is avoided.
4) Independence from the coordinate attached to the object's COM by the task-oriented strategy and formation-based idea facilitates the practical implementation.

It is worth mentioning that the network topology discussed in this paper is directed and contains a spanning tree. From a practical point of view, this topology requires fewer communication links between the robotic agents, which reduces the communication cost and facilitates the network setup, especially in application scenarios involving a large number of robotic agents in manipulation tasks. The presented results also apply to other communication graphs with stronger couplings, for example the balanced and strongly connected graph, undirected and connected graph, etc.

II. Problem Formulation

A. *Preliminaries*

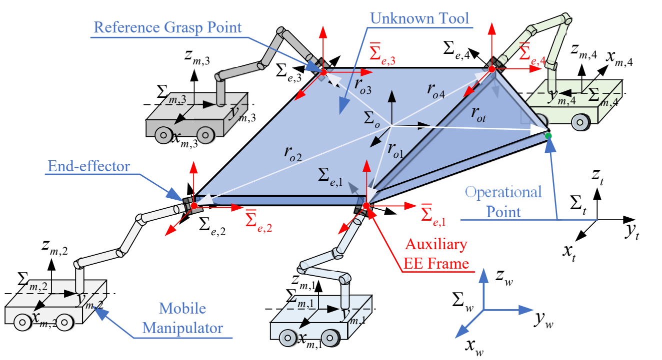

Fig. 1: Networked mobile manipulators cooperatively transporting and manipulating an unknown tool

Consider N mobile manipulators tightly grasping a common unknown object, as shown in Fig. 1. Let $\Sigma_{e,i}$ denote the frame fixed to the end-effector of the ith mobile manipulator. Furthermore, the object frame Σ_o and the cooperative task frame Σ_t are two frames both attached to the object and their origins are chosen so as to coincide with the object's COM and the operational point, respectively. All quantities are expressed with respect to a common world reference frame Σ_w, unless otherwise stated. For each mobile manipulator, the mounted manipulator is considered as a holonomic system while the mobile platform is assumed to be nonholonomic. Throughout this paper, I_m denotes the $m \times m$ identity matrix, $0_{m\times n}$ represents a $m \times n$ null matrix and $0_m = [0, ..., 0]^T \in \mathbb{R}^m$ is a $m \times 1$ column vector with all elements equal to 0. The Cartesian-space variable $x_{\text{sub}} = \left[p_{\text{sub}}^T, o_{\text{sub}}^T\right]^T \in \mathbb{R}^m$ can be split into the translational part $p_{\text{sub}} \in \mathbb{R}^3$ and the rotational part $o_{\text{sub}} \in \mathbb{R}^3$ in the case of $m = 6$. For the trajectory generation of the manipulator system, a Euler angle triplet (RPY) $o_{\text{sub}} = [\varphi_{\text{sub}}, \vartheta_{\text{sub}}, \psi_{\text{sub}}]^T$ is employed to describe the orientation, which enables the specification of a timing law [29]. The matrix $R(o_{\text{sub}})$ represents the rotation of o_{sub} and $o(R_{\text{sub}})$ is the RPY triplet extracted from rotation matrix R_{sub}. Let $\dot{p}_{\text{sub}}$ and ω_{sub} denote the translational and rotational velocity. It should be noted that the twist $v_{\text{sub}} = \left[\dot{p}_{\text{sub}}^T, \omega_{\text{sub}}^T\right]^T \in \mathbb{R}^6$ is related to the time derivative of x_{sub} by $v_{\text{sub}} = T_{A,\text{sub}}\dot{x}_{\text{sub}}$, where the transformation matrix $T_{A,\text{sub}}$ is defined by:

$$
\begin{gathered}
T_{A,\text{sub}} = \operatorname{diag}(I_3, T_{r,\text{sub}}) \\
T_{r,\text{sub}} \triangleq \begin{bmatrix} 0 & -\sin(\varphi_{\text{sub}}) & \cos(\vartheta_{\text{sub}})\cos(\varphi_{\text{sub}}) \\ 0 & \cos(\varphi_{\text{sub}}) & \cos(\vartheta_{\text{sub}})\sin(\varphi_{\text{sub}}) \\ 1 & 0 & -\sin(\vartheta_{\text{sub}}) \end{bmatrix}
\end{gathered}
\tag{1}
$$

TABLE I
NOMENCLATURE

Notation	Definition
$\hat{\text{A}}$	Estimated form of the related matrix/vector A
$\tilde{\text{A}}$	Parameter estimation error of the related matrix/vector A
$\bar{\text{A}}$	The quantity associated with the auxiliary end-effector frame
$T_{A,\text{sub}}$	Block diagonal matrix defined in (1)
$R_{j,i}$	Rotation matrix of $\Sigma_{e,i}$ with respect to $\Sigma_{e,j}$
b_i	Binary variable that defines the accessibility of the desired trajectory to the ith mobile manipulator
q_i	Generalized coordinates of the ith mobile manipulator
ζ_i	Reduced coordinates of the ith mobile manipulator
$x_{e,i}$	End-effector pose vector of the ith mobile manipulator
$J_{e,i}$	Reduced Jacobian matrix of the ith mobile manipulator
$Y_{k,i}$	Kinematic regressor matrix
$\theta_{k,i}$	Linearized kinematic parameters
x_t	Task-space coordinates at the object's operational point
x_{td}	Desired cooperative trajectory
$Y_{d,i}$	Dynamic regressor matrix
$\theta_{d,i}$	Linearized dynamic parameters
$M_{s,i}$	Synthesized inertia matrix of the ith mobile manipulator
$C_{s,i}\dot{\zeta}_i$	Synthesized Coriolis/centrifugal forces of the ith mobile manipulator
$G_{s,i}$	Synthesized gravitational forces of the ith mobile manipulator
$\mathcal{F}_{tr}(t)$	Collective basis function of the desired cooperative task
θ_{tr}	Linearized parameters of the desired cooperative task
δ_i	Allocated task estimation error defined in (20)
γ_i	Consensus error defined in (21)
$\mathcal{T}_{ji}$	Relative displacement and orientation between the jth and the ith end-effectors
$\mathcal{T}_{ti}$	Relative displacement and orientation between the task frame and the ith end-effector
$\dot{x}_{o,i}$	Observed EE velocity defined in (30)
e_i	Cross-coupling error defined in (33)
$S_{x,i}$	Cartesian-space sliding variable defined in (34)
$\dot{\zeta}_{r,i}$	Joint-space reference velocity defined in (35)
$\tilde{x}_{o,i}$	$= x_{o,i} - x_{e,i}$, observer error of the ith mobile manipulator.
$\Delta x_{e,i}$	$= x_{e,i} - \hat{x}_{d,i}$, tracking error of the ith mobile manipulator.
$\Delta x_{o,i}$	$= x_{o,i} - \hat{x}_{d,i}$, error between the observed EE pose and desired EE pose.
$\hat{x}_{d,i}$	Estimated desired trajectory for the ith end-effector
s_i	Joint-space sliding vector defined in (38)
$F_{e,i}$	External wrench exerted by the holonomic constraint on the ith end-effector
$F_{I,i}$	Internal wrench of the ith mobile manipulator
$F_{Id,i}$	Desired internal wrench
$\varepsilon_{d,i}$	Intermediate error variable defined in (19) or (48)
τ_i	Input torques of the ith mobile manipulator

Assumption 1: The unknown object is rigid and the networked mobile manipulators grasp the object tightly so that there is no relative motion between the end-effectors and the object. The multi-arm grasp considered here allows bilateral force and torque transmission [30]. For the cooperative grasp strategy, the readers are referred to [31].

Assumption 2: Each mobile manipulator has access to its end-effector position and the initial position of the operational point. This can be achieved by an external motion capture system in a lab environment or by a local sensor suite [32] for autonomous outdoor tasks.

In the case that the end-effector has a complex mechanical structure, e.g., a dexterous hand, a reference grasp point can be defined at the end-effector as the origin of $\Sigma_{e,i}$. Dynamic and kinematic uncertainties of the end-effector are taken into account as part of the system uncertainties.

B. Kinematics and dynamics of the interconnected system

Denote by $q_i = [q_{v,i}^T, q_{m,i}^T]^T \in \mathbb{R}^{n_r}$ the generalized coordinates of the *i*th mobile manipulator with $q_{v,i} \in \mathbb{R}^{n_v}$ representing the position and orientation of the mobile platform and $q_{m,i} \in \mathbb{R}^{n_m}$ describing the joint angle vector of the mounted manipulator, and $n_r = n_v + n_m$.

The nonholonomic constraint acting on the mobile platform can be expressed as [33]:

$$A_{v,i}(q_{v,i})\dot{q}_{v,i} = 0_{n_c} \tag{2}$$

where $A_{v,i}(q_{v,i}) \in \mathbb{R}^{n_c \times n_v}$ denotes the constraint matrix of the mobile platform. Constraint equation (2) implies that there exists a reduced vector $\zeta_{v,i} \in \mathbb{R}^{n_v - n_c}$, such that

$$\dot{q}_{v,i} = H_{v,i}(q_{v,i})\dot{\zeta}_{v,i} \tag{3}$$

where $H_{v,i}$ satisfies that $H_{v,i}^T(q_{v,i})A_{v,i}^T(q_{v,i}) = 0_{(n_v-n_c)\times n_c}$. Then a reduced vector $\zeta_i = [\zeta_{v,i}^T, q_{m,i}^T]^T \in \mathbb{R}^{n_r - n_c}$ can be defined, which will be used in the sequel.

Let $x_{e,i} \in \mathbb{R}^m$ denote the EE pose vector of *i*th mobile manipulator. It is related to the generalized coordinates by

$$\dot{x}_{e,i} = J_i(q_i)\dot{q}_i = J_{e,i}(\zeta_i)\dot{\zeta}_i \tag{4}$$

where $J_i(q_i) \in \mathbb{R}^{m \times n_r}$ is the whole mobile manipulator Jacobian matrix, $J_{e,i} \in \mathbb{R}^{m \times (n_r - n_c)}$ is the reduced Jacobian matrix that will be defined later, $m \le n_r - n_c$ and equality holds for the non-redundant mobile manipulator.

Property 1: The kinematics (4) linearly depends on a kinematic parameter vector $\theta_{k,i} = [\theta_{k1,i}, ..., \theta_{kp_{k,i},i}]^T \in \mathbb{R}^{p_{k,i}}$, such as joint offsets and link lengths of the manipulator [34]:

$$\dot{x}_{e,i} = J_{e,i}(\zeta_i, \theta_{k,i})\dot{\zeta}_i = Y_{k,i}(\zeta_i, \dot{\zeta}_i)\theta_{k,i} \tag{5}$$

where $Y_{k,i}(\zeta_i, \dot{\zeta}_i) \in \mathbb{R}^{m \times p_{k,i}}$ is the kinematic regressor matrix.

Let $x_{\rm obj} \in \mathbb{R}^m$ be the coordinate vector of the object's COM and it is assumed that $\dot{x}_{\rm obj}$ is related to $\dot{x}_{e,i}$ by

$$T_{A,i}\dot{x}_{e,i} = J_{o,i}T_{A,o}\dot{x}_{\rm obj} \tag{6}$$

where $T_{A,i}$ and $T_{A,o}$ are two transformation matrices defined in (1), $J_{o,i} = [I_3, -S(r_{oi}); 0_{3\times3}, I_3]$ denotes the object Jacobian matrix, $S(\cdot)$ is the skew-symmetric operator and r_{oi} is the vector from the object's COM to the corresponding contact point. Definitions of r_{oi} for $i = 1, 2, ..., N$ are presented in Fig. 1. Here the object's COM is introduced to facilitate the force analysis and will be avoided in the controller design.

Assumption 1 imposes the following kinematic constraints on the relative motion of the attached end-effectors:

$$x_{e,i} = x_{e,j} + \mathcal{T}_{ji} \tag{7}$$

where $\mathcal{T}_{ji} = [(R_{w,i}{}^i r_{ji})^T, {}^w\phi_{ji}^T]^T$ with $R_{w,i}{}^i r_{ji}$ and ${}^w\phi_{ji}$ respectively representing the relative displacement and orientation (represented by the RPY triplet), $R_{w,i}$ is the rotation matrix of $\Sigma_{e,i}$ with respect to Σ_w, ${}^i r_{ji}$ denotes the vector pointing from the *j*th grasp point to the *i*th grasp point expressed in the frame $\Sigma_{e,i}$. To facilitate the implementation of the trajectory estimation in Section III-A, an auxiliary EE frame $\bar{\Sigma}_{e,i}$ is defined for each robot whose axes align with those of the task frame (see Fig. 1). Thus the rotation matrix of $\bar{\Sigma}_{e,i}$ satisfies $\bar{R}_{w,i} = R_{w,t}$ and the pose vector $\bar{x}_{e,i}$ related to $\bar{\Sigma}_{e,i}$ satisfies the constraint $\bar{x}_{e,i} = \bar{x}_{e,j} + \bar{\mathcal{T}}_{ji}$ where $\bar{\mathcal{T}}_{ji} = [(R_{w,i}{}^i r_{ji})^T, 0_3^T]^T$. By exchanging the initial pose through the communication network, ${}^i r_{ji}$ and relative rotation matrix $\bar{R}_{i,i} = \bar{R}_{w,i}^T R_{w,i}$ are assumed to be known to the *i*th robot since they are fixed after the object is grasped. The constraint between $\bar{\Sigma}_{e,i}$ and Σ_t can be expressed in a similar way, i.e., $\bar{x}_{e,i} = x_t + \bar{\mathcal{T}}_{ti}$ with $\bar{\mathcal{T}}_{ti} = [(R_{w,i}{}^i r_{ti})^T, 0_3^T]^T$. Computation of $\mathcal{T}_{ti}$ is similar to that of $\mathcal{T}_{ji}$.

Dynamics of the *i*th mobile manipulator in joint space can be expressed as

$$M_i(q_i)\ddot{q}_i + C_i(q_i, \dot{q}_i)\dot{q}_i + G_i(q_i) = B_i(q_i)\tau_i - A_i^T F_i \tag{8}$$

where $M_i(q_i) = [M_{v,i}, M_{vm,i}; M_{mv,i}, M_{m,i}] \in \mathbb{R}^{n_r \times n_r}$ denotes the symmetric positive definite inertia matrix and $C_i(q_i, \dot{q}_i) = [C_{v,i}, C_{vm,i}; C_{mv,i}, C_{m,i}] \in \mathbb{R}^{n_r \times n_r}$ is the Coriolis and centrifugal matrix, $M_{vm,i}\ddot{q}_{m,i}$ and $M_{mv,i}\ddot{q}_{v,i}$ represent the interaction inertia torques between manipulator and mobile platform, $G_i(q_i) = [G_{v,i}^T, G_{m,i}^T]^T \in \mathbb{R}^{n_r}$ is the gravitational torque vector, $B_i(q_i) = \mathrm{diag}(B_{v,i}, B_{m,i}) \in \mathbb{R}^{n_r \times p}$ is the input transformation matrix for the whole mobile manipulator, $\tau_i = [\tau_{v,i}^T, \tau_{m,i}^T]^T \in \mathbb{R}^p$ denotes the input torques, $F_i = [\lambda_{v,i}^T, (T_{A,i}^T F_{e,i})^T]^T \in \mathbb{R}^{n_c+m}$ in which $\lambda_{v,i} \in \mathbb{R}^{n_c}$ represents the Lagrange multiplier associated with the nonholonomic constraint and $F_{e,i} \in \mathbb{R}^m$ denotes the external wrenches exerted by the holonomic constraint. Moreover, $A_i = [A_{v,i}, 0_{n_c \times n_m}; J_{v,i}, J_{m,i}] \in \mathbb{R}^{(n_c+m)\times n_r}$ in which $J_{v,i}$ and $J_{m,i}$ respectively represent the Jacobian matrices of the mobile base and the manipulator with opportune dimensions.

Considering (3) and its derivative and multiplying both sides of (8) by $\left[H_{v,i}^T, 0_{(n_v-n_c)\times n_m}; 0_{n_m \times n_v}, I_{n_m}\right]$ yields the following reformulation:

$$M_{r,i}\ddot{\zeta}_i + C_{r,i}\dot{\zeta}_i + G_{r,i} = B_{r,i}\tau_i - J_{e,i}^T T_{A,i}^T F_{e,i} \tag{9}$$

where $M_{r,i}$, $B_{r,i}$, $C_{r,i}$ and $G_{r,i}$ are given in Appendix A. Then the nonholonomic constraint force $A_{v,i}^T \lambda_{v,i}$ in (8) can be eliminated; $J_{e,i} = [J_{v,i}H_{v,i}, J_{m,i}] \in \mathbb{R}^{m \times (n_r - n_c)}$.

Dynamics of the grasped object can be described by:

$$M_o(x_{\rm obj})\dot{v}_{\rm obj} + C_o(x_{\rm obj}, \dot{x}_{\rm obj})v_{\rm obj} + g_o(x_{\rm obj}) = F_o \tag{10}$$

where $v_{\rm obj} \in \mathbb{R}^m$ is the velocity of the object and it is related to $\dot{x}_{\rm obj}$ by $v_{\rm obj} = T_{A,o}\dot{x}_{\rm obj}$, $M_o(x_{\rm obj}) \in \mathbb{R}^{m \times m}$ denotes the inertia matrix and is assumed to be bounded and symmetric positive definite, $\lambda_{o,\min} I_m \le M_o \le \lambda_{o,\max} I_m$, where $\lambda_{o,\min}$ and $\lambda_{o,\max}$ represent the minimum and maximum eigenvalues of M_o, $C_o(x_{\rm obj}, \dot{x}_{\rm obj})$ is the $m \times m$ Coriolis and centrifugal matrix and $g_o(x_{\rm obj}) \in \mathbb{R}^m$ represents the gravitational vector, $F_o \in \mathbb{R}^m$ is the resultant wrench acting on the object's COM by the multiple mobile manipulator ensemble.

By virtue of kineto-statics duality, the resultant wrench F_o acting on the object's COM satisfies the following relation:

$$F_o = G_o F_e \tag{11}$$

where $G_o = J_o^T = [J_{o,1}^T, J_{o,2}^T, ..., J_{o,N}^T] \in \mathbb{R}^{m \times Nm}$ is the well-known grasp matrix, $F_e = [F_{e,1}^T, F_{e,2}^T, ..., F_{e,N}^T]^T \in \mathbb{R}^{Nm}$ is the collective vector consisting of all generalized wrenches exerted by the mobile manipulators on the object, which can be measured by the force/torque sensor mounted at the wrist of each manipulator. F_o can also be expressed as $F_o = \sum_{i=1}^{N} F_{ce,i}$, where $F_{ce,i} = J_{o,i}^T F_{e,i}$ is the wrench indirectly applied on the object's COM by the ith end-effector, and can be decomposed into two orthogonal components: one is the manipulation wrench $F_{E,i} \in \mathbb{R}^m$ which contributes to the motion of the grasped object, the other one is the internal wrench $F_{I,i} \in \mathbb{R}^m$ which contributes to the build-up of the stress in the object. This relation can be expressed as: $F_{ce,i} = F_{E,i} + F_{I,i}$ with $\sum_{i=1}^{N} F_{I,i} = 0_m$.

Suppose that a desired load distribution among the robot team is described by a set of positive definite diagonal matrices $\beta_i(t) \in \mathbb{R}^{m\times m}$ for $i = 1, 2, ..., N$ with the assumption that $\|\dot{\beta}_i(t)\| \leq d_i$ (d_i is a positive constant) [35]:

$$F_{E,i} = \beta_i(t)[M_o(x_{\text{obj}})\dot{\upsilon}_{\text{obj}} + C_o(x_{\text{obj}}, \dot{x}_{\text{obj}})\upsilon_{\text{obj}} + g_o(x_{\text{obj}})] \tag{12}$$

A physical property regarding the load distribution matrices is that $\sum_{i=1}^{N} \beta_i(t) = I_m$. Then incorporating (12) and above-mentioned properties into (9) gives the dynamics of the interconnected system in a distributed fashion:

$$M_{s,i}\ddot{\zeta}_i + C_{s,i}\dot{\zeta}_i + G_{s,i} = B_{r,i}\tau_i - J_{\phi,i}^T F_{I,i} \tag{13}$$

where

$$\begin{aligned} M_{s,i} &= M_{r,i} + \beta_i(t) J_{\phi,i}^T M_o J_{\phi,i}, \\ C_{s,i} &= C_{r,i} + \beta_i(t)[J_{\phi,i}^T C_o J_{\phi,i} + J_{\phi,i}^T M_o \frac{dJ_{\phi,i}}{dt}], \\ G_{s,i} &= G_{r,i} + \beta_i(t) J_{\phi,i}^T g_o, \quad J_{\phi,i} = J_{o,i}^{\dagger} T_{A,i} J_{e,i}. \end{aligned}$$

Property 2: The matrix $\dot{M}_{s,i} - 2C_{s,i} - \dot{\beta}_i J_{\phi,i}^T M_o J_{\phi,i}$ is skew symmetric so that $\upsilon^T[\dot{M}_{s,i} - 2C_{s,i} - \dot{\beta}_i J_{\phi,i}^T M_o J_{\phi,i}]\upsilon = 0$ for all $\upsilon \in \mathbb{R}^{(n_r - n_c)}$, see Appendix A for the proof.

Then the following inequality holds since the robots work in finite joint space

$$\left\|\dot{\beta}_i J_{\phi,i}^T M_o J_{\phi,i}\right\| \leq d_i \lambda_{o,\max} \left\|J_{\phi,i}^T J_{\phi,i}\right\| = \vartheta_i \tag{14}$$

where ϑ_i is a positive constant that denotes the upper bounds of $\|\dot{\beta}_i J_{\phi,i}^T M_o J_{\phi,i}\|$.

Property 3: The nonlinear dynamics linearly depends on a dynamic parameter vector $\theta_{d,i} = [\theta_{d1,i}, ..., \theta_{dp_{d,i},i}]^T \in \mathbb{R}^{p_{d,i}}$ which is composed of physical parameters of the object and the mobile manipulator, which gives rise to

$$M_{s,i}\ddot{\zeta}_i + C_{s,i}\dot{\zeta}_i + G_{s,i} = Y_{d,i}(\zeta_i, \dot{\zeta}_i, \ddot{\zeta}_i, \beta_i)\theta_{d,i} \tag{15}$$

where $Y_{d,i}(\zeta_i, \dot{\zeta}_i, \ddot{\zeta}_i, \beta_i)$ is the dynamic regressor matrix.

Remark 1. To avoid input transformation uncertainty which is associated with kinematic uncertainty of the mobile base, ζ_i can be defined to coincide with the actuation space of the mobile manipulator, i.e., $\zeta_i = [q_{R,i}, q_{L,i}, q_{m1,i}, ...q_{mn_ri}]^T$ for a two-wheel mobile platform where $q_{R,i}$ and $q_{L,i}$ are the two independent driving wheels. Thus, $B_{r,i} = I_{(n_r - n_c)}$ and the uncertainties in the input transformation matrix are eliminated.

C. Communication topology

As is commonly done in distributed control, a graph $\mathcal{G} = (\mathcal{V}, \mathcal{E})$ is employed here to describe the communication topology among the N mobile manipulators where the vertex set $\mathcal{V} = \{1, 2, ..., N\}$ represents all the robots in the network and the edge set $\mathcal{E} \subseteq \mathcal{V} \times \mathcal{V}$ denotes the communication interaction between the robots. The edge (i, j) in the directed graph indicates that robot i can receive information from robot j but not vice versa. Neighbors of robot i form a set $\mathcal{N}_i = \{j|(i,j) \in \mathcal{E}, j \in \mathcal{V}\}$. The $N \times N$ adjacency matrix $\mathcal{A} = [a_{ij}]$ associated with this graph is defined as $a_{ij} = 1$ if $j \in \mathcal{N}_i$ and $a_{ij} = 0$ otherwise. Additionally, self-loops are not contained, i.e., $a_{ii} = 0$. Then the Laplacian matrix $\mathcal{L} = [l_{ij}] \in \mathbb{R}^{N\times N}$ can be defined as

$$l_{ij} = \begin{cases} \sum_{k=1}^{N} a_{ik} & \text{if } i = j \\ -a_{ij} & \text{otherwise} \end{cases} \tag{16}$$

Assumption 3: In this paper, the graph that the N mobile manipulators interact on is directed with a spanning tree whose root node has direct access to the desired trajectory of the operational point, i.e., x_{td}.

This assumption implies that only a small subset of the robotic agents has direct access to the desired cooperative trajectory x_{td}. It is a more general case with less restrictions in real application scenarios, yet, may complicate the controller design since the agents that cannot obtain x_{td} should estimate it to achieve the cooperative task by utilizing only locally available signals. A binary variable b_i is defined here to indicate the accessibility of x_{td} and $b_i = 1$ if the ith robotic agent has access to $x_{t,d}$, otherwise b_i is set to 0.

Several properties of the Laplacian matrix associated with the graph in Assumption 3 are listed in the following lemma.

Lemma 1: The matrix $(\mathcal{L} + \mathcal{B})$ with $\mathcal{B} = \text{diag}\,(b_1, ..., b_N)$ is nonsingular. Define $w = [w_1, ..., w_N]^T = (\mathcal{L} + \mathcal{B})^{-1} 1_N$ and $\mathcal{P} = \text{diag}\,(\mathcal{P}_1, ..., \mathcal{P}_N) = \text{diag}\,(1/w_1, ..., 1/w_N)$, then $\mathcal{Q} = \mathcal{P}\,(\mathcal{L} + \mathcal{B}) + (\mathcal{L} + \mathcal{B})^T \mathcal{P}$ is positive definite [36].

Based on the models, assumptions and interaction topology discussed above, the control objective is to design a set of distributed controllers τ_i for the multiple mobile manipulator system to cooperatively transport an object irrespective of uncertain dynamics and interconnected kinematics such that:

1) The operational point on the manipulated object could track a desired designated trajectory.
2) Task allocation and motion tracking of the networked mobile manipulators are synchronized.
3) All the signals in the closed-loop interconnected system remain bounded.

III. Distributed Adaptive Cooperation

This section is devoted to the formulation of the fully distributed cooperation scheme, whose main structure is shown in Fig. 2. To enable the networked robotic system to perform a tight cooperation task, i.e., object transportation/manipulation discussed in this paper, the cooperative task should be well allocated to every agent in a distributed way. In addition, internal wrench regulation and motion tracking control of each agent in the presence of kinematic/dynamic uncertainties both need detailed investigation. Discussions of these three topics constitute the proposed scheme and are respectively presented in the following subsections.

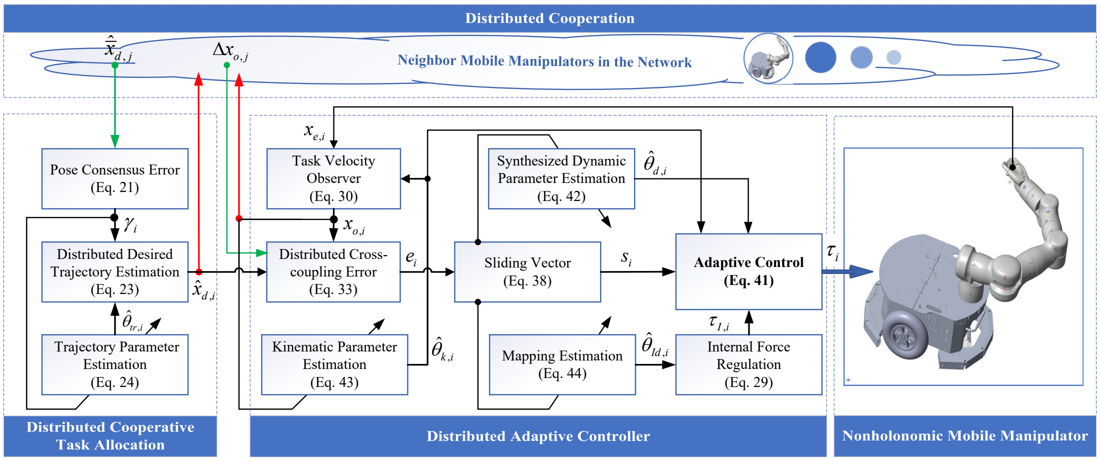

Fig. 2: Fully distributed cooperation scheme for the networked mobile manipulator

A. Distributed cooperative task allocation

To achieve motion tracking control of the operational point, the task allocation for the end-effector of each mobile manipulator under limited communication can be interpreted as a rigid formation control problem, i.e., the operational point can be treated as a virtual leader that generates a desired trajectory and virtual followers are associated with the mobile manipulators that should be controlled to maintain the rigid formation in consideration of the rigid grasp. This means the desired local trajectory $x_{d,i}$ ($\bar{x}_{d,i}$ for auxiliary frame) of the ith robotic agent should satisfy the kinematic constraint $x_{d,i} = x_{td} + \mathcal{T}_{ti}$ ($\bar{x}_{d,i} = x_{td} + \bar{\mathcal{T}}_{ti}$).

A continuous function usually can be approximated by a linear combination of a set of prescribed basis functions [37], i.e., $f(t) = \sum_{k=1}^{l} f_{tr,k}(t)\, \Theta_{tr,k}$. Then, the desired trajectory for the operational point of the grasped object $x_{td} = [p_{td}^T, o_{td}^T]^T$ can be represented as

$$\begin{aligned} x_{td} &= \left[\mathcal{F}_{tr}(t)\, \bar{\Theta}_{tr,1}, ..., \mathcal{F}_{tr}(t)\, \bar{\Theta}_{tr,m}\right]^T \\ &= \begin{bmatrix} (I_3 \otimes \mathcal{F}_{tr}(t))\, \theta_{tr,p} \\ (I_3 \otimes \mathcal{F}_{tr}(t))\, \theta_{tr,o} \end{bmatrix} = (I_6 \otimes \mathcal{F}_{tr}(t))\, \theta_{tr} \end{aligned} \tag{17}$$

where $\mathcal{F}_{tr}(t) = [f_{tr,1}, f_{tr,2}, ..., f_{tr,l}] \in \mathbb{R}^l$ is the collective basis function that is assumed to be known to all robotic agents, $\bar{\Theta}_{tr,i} = [\Theta_{tr,i,1}, ..., \Theta_{tr,i,l}]^T \in \mathbb{R}^l$ is the constant parameter vector for the ith component of x_{td}, $\theta_{tr} = [\theta_{tr,p}^T, \theta_{tr,o}^T]^T = [\bar{\Theta}_{tr,1}^T, ..., \bar{\Theta}_{tr,m}^T]^T \in \mathbb{R}^{lm}$ denotes the constant parameters and $\otimes$ is the Kronecker product. Only the root robotic agent has access to x_{td}, the others need to estimate the unknown θ_{tr} to reconstruct the desired trajectory based on locally available information. This statement coincides with Assumption 3 and the definition of the matrix $\mathcal{B}$.

Remark 2. It is reasonable to approximate the desired trajectories by employing (17), especially in the context of the robot trajectory planning, since the interpolating functions of the desired trajectories are typically specified as polynomials to guarantee continuity of the velocity and acceleration [29]. For a more general case in which the desired trajectory is continuous but arbitrary, a neural network can be utilized to approximate this trajectory based on its universal approximation theorem [38]. In both cases, $\mathcal{F}_{tr}$ is smooth and of class $\mathcal{C}_\infty$.

Instead of directly estimating $x_{d,i}$, $\bar{x}_{d,i}$ is estimated here. Let $\hat{\bar{x}}_{d,i} = [\hat{\bar{p}}_{d,i}^T, \hat{\bar{o}}_{d,i}^T]^T$ and $\hat{x}_{d,i} = [\hat{p}_{d,i}^T, \hat{o}_{d,i}^T]^T$ be the distributed estimation of the desired trajectory allocated to $\bar{\Sigma}_{e,i}$ and $\Sigma_{e,i}$. Then $\hat{x}_{d,i}$ can be directly calculated by using the following rigid transformation:

$$\begin{cases} \hat{p}_{d,i} = \hat{\bar{p}}_{d,i} \\ \hat{o}_{d,i} = o(R(\hat{\bar{o}}_{d,i})\bar{R}_{i,i}) \end{cases} \tag{18}$$

To facilitate the distributed estimation of the desired trajectory, the following two error variables are defined:

$$\begin{aligned} \varepsilon_{d,i} =& -(1-b_i)\left[(I_6 \otimes \mathcal{F}_{tr}(t))\hat{\theta}_{tr,i} + \hat{\bar{\mathcal{T}}}_{ti}(\hat{o}_{d,i})\right] \\ &+ \hat{\bar{x}}_{d,i} - b_i(x_{td} + \bar{\mathcal{T}}_{ti}) \end{aligned} \tag{19}$$

$$\delta_i = \hat{\bar{x}}_{d,i} - \bar{\mathcal{T}}_{ti} - x_{td} \tag{20}$$

where $\varepsilon_{d,i} = [\varepsilon_{pd,i}^T, \varepsilon_{od,i}^T]^T$ is an intermediate error variable which is defined to facilitate the convergence analysis, $\delta_i = [\delta_{p,i}^T, \delta_{o,i}^T]^T$ denotes the actual estimation error between the desired local trajectory and its estimation, $\hat{\theta}_{tr,i} = [\hat{\theta}_{tr,p,i}^T, \hat{\theta}_{tr,o,i}^T]^T$ is the estimate of the trajectory parameter vector θ_{tr} by the ith mobile manipulator, $\hat{\bar{\mathcal{T}}}_{ti}$ is the estimate of $\bar{\mathcal{T}}_{ti}$ and can be computed by substituting $\hat{o}_{d,i}$ into its expression $[(\hat{R}_{w,i}(\hat{o}_{d,i})^i r_{ti})^T, 0_3^T]^T$. Then, the ideal cooperative task allocation under a rigid grasp condition can be interpreted as $\hat{\bar{x}}_{d,i} \to \bar{x}_{d,i}$, i.e., $\delta_i \to 0$.

To achieve our control objective, the definition of standard local neighborhood consensus error [39] is redesigned as:

$$\begin{aligned} \gamma_i =& \sum_{j \in \mathcal{N}_i} \left[\hat{\bar{x}}_{d,i} - \hat{\bar{x}}_{d,j} - b_i\bar{\mathcal{T}}_{ji} - (1-b_i)\hat{\bar{\mathcal{T}}}_{ji}\right] \\ &+ b_i(\hat{\bar{x}}_{d,i} - \bar{\mathcal{T}}_{ti} - x_{td}) \end{aligned} \tag{21}$$

where $\hat{\bar{\mathcal{T}}}_{ji}$ is the estimate of $\bar{\mathcal{T}}_{ji}$ and can be obtained by substituting $\hat{o}_{d,i}$ into its expression $[(\hat{R}_{w,i}(\hat{o}_{d,i})^i r_{ji})^T, 0_3^T]^T$, $\gamma_i = [\gamma_{p,i}^T, \gamma_{o,i}^T]^T$ can be split into $\gamma_{p,i} \in \mathbb{R}^3$ and $\gamma_{o,i} \in \mathbb{R}^3$. Since $\bar{\mathcal{T}}_{ji} = [(R_{w,i}(o_{d,i})^i r_{ji})^T, 0_3^T]^T$ is associated with $o_{d,i}$, $\bar{\mathcal{T}}_{ji}$ is also not available to the robotic agents with $b_i = 0$ and should be replaced by its estimation. The two terms $b_i\bar{\mathcal{T}}_{ji}$

and $(1-b_i)\hat{\bar{\mathcal{T}}}_{ji}$ in (21) are mutually exclusive, thus γ_i only depends on locally available signals.

Together with (20), (21) can be reformulated as:

$$\gamma_i = \sum_{j\in\mathcal{N}_i}\left[\delta_i - \delta_j - (1-b_i)\tilde{\mathcal{T}}_{ji}\right] + b_i\delta_i \tag{22}$$

where $\tilde{\mathcal{T}}_{ji} = \hat{\bar{\mathcal{T}}}_{ji} - \bar{\mathcal{T}}_{ji} = [((\hat{R}_{w,i} - R_{w,i})^i r_{ji})^T, 0_3^T]^T$ is the estimation error of $\bar{\mathcal{T}}_{ji}$.

Then, the distributed estimation law of the local desired trajectory and its parameter update law are proposed as:

$$\begin{aligned}\dot{\hat{\bar{x}}}_{d,i} =& -\kappa\mathcal{P}_i\gamma_i + b_i\left[(I_6\otimes\dot{\mathcal{F}}_{tr})\theta_{tr} + \dot{\bar{\mathcal{T}}}_{ti}\right] \\ &+ (1-b_i)\left[(I_6\otimes\mathcal{F}_{tr})\dot{\hat{\theta}}_{tr,i} + (I_6\otimes\dot{\mathcal{F}}_{tr})\hat{\theta}_{tr,i}\right] \\ &+ (1-b_i)\,\dot{\hat{\bar{\mathcal{T}}}}_{ti}(\hat{o}_{d,i},\hat{\omega}_{d,i})\end{aligned} \tag{23}$$

$$\dot{\hat{\theta}}_{tr,i} = -\Gamma_{tr,i}(I_6\otimes\mathcal{F}_{tr}(t))^T\gamma_i \qquad \text{for } b_i = 0 \tag{24}$$

where κ and $\Gamma_{tr,i}$ are positive constants, $\dot{\bar{\mathcal{T}}}_{ti}$ is the derivative of $\bar{\mathcal{T}}_{ti}$ and is equal to $[(S(\omega_{d,i})R_{w,i}{}^i r_{ti})^T, 0_3^T]^T$, $\omega_{d,i}$ denotes the first derivative of $o_{d,i}$ and this nomenclature applies to the definition of $\hat{\omega}_{d,i}$ and $\hat{o}_{d,i}$, γ_i in these two equations is obtained by using (21).

Remark 3. It should be noted that pose (including the position and orientation) formation tracking control is achieved here, which distinguishes the proposed estimation/update law from the standard consensus error defined in [39].

Remark 4. Unlike other decentralized or distributed schemes [24], [35] in which the desired cooperative trajectory for each robotic agent is assumed to be known to all, only locally available signals are utilized in (21), (23) and (24), thus endowing the whole mobile manipulator ensemble with the ability to work in a fully distributed way. Furthermore, the proposed estimation law does not require any persistent excitation condition of the desired trajectory and is independent from the frame of the object's COM. These two significant properties that are also the objectives pursued through the following adaptive control design facilitate the whole scheme's practical implementation.

B. Internal wrench regulation

This subsection mainly concerns the physically plausible wrench synthesis scheme based on which the internal wrench regulation law is presented. Before formulating the distributed internal wrench regulation, three constraints that a physically plausible internal wrench must obey are presented first [40]:

$$\begin{aligned}\left\|\bar{f}_{I,i}\right\|^2 &\le \bar{f}_{s,i}^T\bar{f}_{I,i} \\ \left\|\bar{\tau}_{fI,i}\right\|^2 &\le \bar{\tau}_{sf,i}^T\bar{\tau}_{fI,i} \\ \left\|\bar{\tau}_{I,i}\right\|^2 &\le \bar{\tau}_{s,i}^T\bar{\tau}_{I,i}\end{aligned} \tag{25}$$

where $\bar{F}_{I,i} = [\bar{f}_{I,i}^T, \bar{\tau}_{I,i}^T]^T$ is the internal wrench mapped to the contact point, $\bar{F}_{s,i} = [\bar{f}_{s,i}^T, \bar{\tau}_{s,i}^T]^T$ denotes the wrench sensed by the force/torque sensor mounted on the *i*th manipulator and it is equivalent to the interaction wrench $F_{e,i}$. The torque $\bar{\tau}_{sf,i}$ is induced by $\bar{f}_{s,i}$ and $\bar{\tau}_{fI,i}$ denotes component internal torque induced by $\bar{f}_{I,i}$.

Extracting the internal wrench component from the interaction wrench (Wrench Decomposition) needs full contact wrench information and thus is inherently centralized. However, definition of the internal wrench is still a controversial research topic in multi-arm cooperation. Instead of using the typical wrench decomposition schemes [11], [40]–[44], wrench synthesis is investigated here to achieve internal wrench regulation and physical constraints are taken into account.

Although it is in general not possible to achieve full decomposition of interactions into internal wrenches leading to wrenches compensating each other and manipulation wrenches contributing to the resultant wrench only without compensating parts [45], the idea of a non-squeezing pseudoinverse [41] can be employed in the wrench synthesis problem here, based on which a more general formulation with non-squeezing effect in the desired manipulation wrenches will be presented. Regarding physical plausibility, the desired internal wrench cannot be arbitrary assigned once the desired load distribution is given. To avoid virtual wrenches that may appear in most of the internal wrench regulation schemes, the wrench decomposition constraints in wrench analysis are further incorporated in our proposed wrench synthesis.

To achieve a desired grasp, the desired manipulation wrench can be given as

$$\bar{F}_{Ed,i} = \begin{bmatrix}\beta_i I_3 & 0_{3\times3} \\ -\beta_i S(r_{oi}) & \beta_i I_3\end{bmatrix} F_{od} \tag{26}$$

where $F_{od} = [f_{od}^T, \tau_{od}^T]^T$ is the desired net wrench that should be applied to the object's COM, $\bar{F}_{Ed,i}$ denotes the desired manipulation wrench mapped to the contact point. With (26), $J_{o,i}^T\bar{F}_{ed,i} = \beta_i F_{od}$ is achieved, thus the desired manipulation wrenches have no internal loading component. As to wrench synthesis, there is no need to keep consistency of the pseudoinverse matrix utilized in the manipulation wrench and internal wrench, which leads to a more general synthesis formulation.

In this way, designation of the desired manipulation wrench and internal wrench for each mobile manipulator is completely decoupled, which contributes to the reduction in the number of constraint equations and the ease of implementation. The constraints imposed on desired load distribution and desired internal wrench are reformulated as the following inequalities in terms of the wrench synthesis:

$$\begin{cases}(\beta_i f_{od})^T f_{Id,i} \ge 0 \\ (\beta_i S(r_{oi})f_{od} - \beta_i\tau_{od})^T\left(S(r_{oi})f_{Id,i} - \tau_{Id,i}\right) \ge 0\end{cases} \tag{27}$$

where $F_{Id,i} = [f_{Id,i}^T, \tau_{Id,i}^T]^T$ is the desired internal wrench.

The following linearization is introduced to facilitate the internal wrench regulation:

$$J_{\phi,i}^T F_{Id,i} = Y_{Id,i}(\zeta_i, F_{Id,i})\theta_{Id,i} \tag{28}$$

where $Y_{Id,i}(\zeta_i, F_{Id,i}) \in \mathbb{R}^{(n_r-n_c)\times p_{Id,i}}$ is the regressor matrix associated with the desired internal wrench and $\theta_{Id,i} = [\theta_{Id,1,i}, \ldots, \theta_{Id,p_{Id,i},i}]^T$ is the linearized parameters.

The internal wrench regulation law $\tau_{I,i}$, that will be used in (41), can be given as:

$$\tau_{I,i} = \hat{J}_{\phi,i}^T F_{Id,i} + \tau_{r,i} \tag{29}$$

where $\hat{J}^T_{\phi,i}$ is the estimate of the Jacobian matrix transpose $J^T_{\phi,i}$ and can be computed by substituting $\hat{\theta}_{Id,i}$ into its expression, $\tau_{r,i} = -k_{r,i}\hat{J}^T_{e,i}\hat{J}_{e,i}s_i$ is the robust term and $k_{r,i}$ is a dynamically regulated positive gain whose range will be given in the sequel.

Remark 5. With (29), the internal wrench tracking error only approaches to a neighborhood of the zero point if the persistent excitation condition is not satisfied. This is acceptable in most applications, especially for the multi-arm grasp, since the internal wrench is only required to be regulated around a constant value to either avoid excessive stress or provide sufficient grasp force [46].

Remark 6. The decentralized schemes in the related literature that cope with the internal wrench regulation can be classified into two categories. In the first one [35], [47], the robotic agents cannot communicate with each other but are assumed to have access to the global force information, so these schemes can only be termed as semi-decentralized schemes. The other approach [22] uses the moment-based observer to estimate the net wrench acting on the grasped object exerted by the mobile manipulator ensemble. However, this is not applicable to our case because it requires the accurate dynamics and kinematics of the grasped object. Different from the above-mentioned works in which internal force is calculated or estimated in a centralized way and an extra integral feedback of the internal force is applied to reduce the overshoot and limit the upper bound of the interaction force, we adopt the synchronization mechanism and small control gains instead. To maintain high tracking performance under multiple uncertainties even with small gains, adaptability studied in the next subsection is effective. This compromise endows the scheme with an attractive attribute that calculation of the internal force is avoided, thus maintaining the distributed manner of the whole scheme. For the tight connection case considered in this paper, the internal wrench should be bounded as small as possible to avoid potential damage to the whole system, i.e., $F_{Id,i} = 0_m$.

C. Distributed adaptive control

In this section, a distributed adaptive control is presented to achieve allocated task tracking and task motion synchronization of the interconnected multiple mobile manipulator under uncertain kinematics and dynamics. This can be interpreted as $\Delta x_{e,i}, \Delta\dot{x}_{e,i} \to 0$ and $\Delta x_{e,i} - \Delta x_{e,j}, \Delta\dot{x}_{e,i} - \Delta\dot{x}_{e,j} \to 0$ after $\delta_i \to 0$, where $\Delta x_{e,i} = x_{e,i} - \hat{x}_{d,i}$ denotes the Cartesian-space tracking error of the *i*th mobile manipulator. Different from state-of-the-art works [22], [27], motion synchronization should be achieved here to alleviate the transient performance degradation since multiple uncertainties exist in our case and the mobile manipulator ensemble is tightly interconnected through the object.

To avoid the noisy Cartesian-space velocities, a distributed observer is presented as follows [48]:

$$\dot{x}_{o,i} = \hat{\dot{x}}_{e,i} - \alpha_i(x_{o,i} - x_{e,i}) \tag{30}$$

where $\dot{x}_{o,i} \in \mathbb{R}^m$ denotes the observed Cartesian-space velocity and α_i is a positive constant, $x_{e,i}$ is provided by Assumption 2. In the presence of kinematic uncertainties, the estimated Cartesian-space velocity $\hat{\dot{x}}_{e,i} \in \mathbb{R}^m$ can be expressed by

$$\hat{\dot{x}}_{e,i} = \hat{J}_{e,i}(\zeta_i, \hat{\theta}_{k,i})\dot{\zeta}_i = Y_{k,i}(\zeta_i, \dot{\zeta}_i)\hat{\theta}_{k,i} \tag{31}$$

where $\hat{\theta}_{k,i}$ is the estimated kinematic parameter vector and $\hat{J}_{e,i}(\zeta_i, \hat{\theta}_{k,i})$ is the estimated Jacobian matrix.

Substituting (31) into (30) and using (4) yields the following closed-loop dynamics of the observer:

$$\dot{\tilde{x}}_{o,i} = -\alpha_i\tilde{x}_{o,i} + Y_{k,i}(\zeta_i, \dot{\zeta}_i)\tilde{\theta}_{k,i} \tag{32}$$

where $\tilde{x}_{o,i} = x_{o,i} - x_{e,i}$ denotes the observer error and $\tilde{\theta}_{k,i} = \hat{\theta}_{k,i} - \theta_{k,i}$ is the estimation error of the linearized kinematic parameters.

To achieve both task tracking objective of each robot and synchronization objective among the robots, we first define a novel cross-coupling error $e_i \in \mathbb{R}^m$

$$e_i = \Delta x_{o,i} + \sum_{j\in\mathcal{N}_i}\int_0^t \varepsilon_i(\Delta x_{o,i} - \Delta x_{o,j}) \tag{33}$$

where $\Delta x_{o,i} = x_{o,i} - \hat{x}_{d,i} \in \mathbb{R}^m$ and ε_i is a positive constant.

Remark 7. Inspired by the centralized cross-coupling error proposed in [49], (33) further takes the communication constraints into consideration and employs the observer error instead of tracking error to achieve distributed control in the presence of kinematic uncertainties.

Remark 8. Motion synchronization of the networked robotic agents is achieved here through explicit convergence of the distributed coupling error, which strikes a balance between the synchronization behavior and the separation property suggested in [50], [51].

Then, define a Cartesian-space sliding variable $S_{x,i} \in \mathbb{R}^m$

$$S_{x,i} = \dot{e}_i + \Lambda_i e_i \tag{34}$$

where $\dot{e}_i$ is the time derivative of cross-coupling error e_i and Λ_i is the adjustable positive diagonal matrix.

Considering the control objectives, the joint-space reference velocity $\dot{\zeta}_{r,i} \in \mathbb{R}^{(n_r-n_c)}$ for the *i*th mobile manipulator is defined as

$$\begin{aligned}\dot{\zeta}_{r,i} =& \hat{J}^{\dagger}_{e,i}(\zeta_i, \hat{\theta}_{k,i})\overbrace{[\hat{\dot{x}}_{d,i} - \sum_{j\in\mathcal{N}_i}\varepsilon_i(\Delta x_{o,i} - \Delta x_{o,j}) - \Lambda_i e_i]}^{\dot{x}_{pr,i}} \\ &+ \underbrace{\hat{N}_{e,i}(\hat{J}_{s,i}\hat{N}_{e,i})^{\dagger}(\dot{x}_{sr,i} - \hat{J}_{s,i}\hat{J}^{\dagger}_{e,i}\dot{x}_{pr,i})}_{\dot{\zeta}_{sr,i}}\end{aligned} \tag{35}$$

where $\hat{N}_{e,i}(\zeta_i, \hat{\theta}_{k,i}) = I_{(n_r-n_c)} - \hat{J}^{\dagger}_{e,i}\hat{J}_{e,i}$ denotes the null-space projector of the estimated Jacobian matrix $\hat{J}_{e,i}$ and $\hat{J}^{\dagger}_{e,i}(\zeta_i, \hat{\theta}_{k,i}) \in \mathbb{R}^{(n_r-n_c)\times m}$ the pseudoinverse. These three matrices can be computed by substituting $\hat{\theta}_{k,i}$ into their respective expressions, $\dot{x}_{pr,i}$ is the task-space reference velocity. The desired local subtask, denoted by $x_{sr,i}$, is implemented by utilizing the redundancy of the *i*th mobile manipulator. The matrices $\hat{J}_{s,i}$ and $(\hat{J}_{s,i}\hat{N}_{e,i})$ denote the estimated subtask Jacobian and the projected Jacobian, respectively. Definition of $\dot{\zeta}_{r,i}$ employs the multi-priority framework to maintain the designated task priorities under kinematic uncertainties.

A modified singularity robust technique [52] can be adopted here to avoid potential singularity of the estimated kinematics and minimize the reconstruction error as far as possible.

$$\begin{aligned}\hat{J}_{e,i}^{\dagger}(\zeta_i,\hat{\theta}_{k,i}) &= \sum\nolimits_{k=1}^{n_{ns,i}} \frac{\sigma_{ik}}{\sigma_{ik}^2+\lambda_{Gik}^2}\nu_{ik}\mu_{ik}^T \\ \lambda_{Gik} &= \lambda_{\max,i}\exp(-(\sigma_{ik}/\Delta_i)^2)\end{aligned} \tag{36}$$

where σ_{ik} is the kth singular value of the estimated Jacobian $\hat{J}_{e,i}$, ν_{ik} and μ_{ik} denote the kth output and input singular vectors, $n_{ns,i}$ is the number of non-null singular value of $\hat{J}_{e,i}$. The design constant Δ_i sets the size of the singularity region and $\lambda_{\max,i}$ denotes the maximum of the damping factor. This technique is also used to avoid the algorithmic singularity of the projected Jacobian.

Differentiating (35) with respect to time leads to the following reference acceleration

$$\begin{aligned}\ddot{\zeta}_{r,i} = \hat{J}_{e,i}^{\dagger}[\ddot{x}_{d,i} - \sum_{j\in\mathcal{N}_i}\varepsilon_i(\Delta\dot{x}_{o,i}-\Delta\dot{x}_{o,j}) - \Lambda_i\dot{e}_i] + \frac{d\dot{\zeta}_{sr,i}}{dt} \\ +\dot{\hat{J}}_{e,i}^{\dagger}[\dot{x}_{d,i} - \sum_{j\in\mathcal{N}_i}\varepsilon_i(\Delta x_{o,i}-\Delta x_{o,j}) - \Lambda_i e_i]\end{aligned} \tag{37}$$

where $\ddot{x}_{d,i}$ represents the desired Cartesian-space acceleration of the ith manipulator. Instead of differentiating $\dot{x}_{d,i}$, $\ddot{x}_{d,i}$ is obtained by using the derivative function of (23) and the rigid transformation (18) to avoid potential noise introduced in the numerical differentiation.

With the reference velocity defined by (35), a joint-space sliding vector $s_i \in \mathbb{R}^{(n_r-n_c)}$ is defined as follows

$$s_i = \dot{\zeta}_i - \dot{\zeta}_{r,i} \tag{38}$$

Incorporating (38) and (35) into (34) yields the following relation between the joint-space velocity and the Cartesian-space sliding vector

$$\hat{J}_{e,i}s_i = S_{x,i} + Y_{k,i}\tilde{\theta}_{k,i} - \dot{\tilde{x}}_{o,i} \tag{39}$$

Considering (15) and substituting (38) with its time derivative into (13) yields

$$M_{s,i}\dot{s}_i + C_{s,i}s_i = \tau_i - J_{\phi,i}^T F_{I,i} - Y_{d,i}(\zeta_i,\dot{\zeta}_i,\dot{\zeta}_{r,i},\ddot{\zeta}_{r,i},\beta_i)\theta_{d,i} \tag{40}$$

Now we propose the adaptive control law for the ith mobile manipulator as

$$\begin{aligned}\tau_i =& \tau_{I,i} + Y_{d,i}(\zeta_i,\dot{\zeta}_i,\dot{\zeta}_{r,i},\ddot{\zeta}_{r,i},\beta_i)\hat{\theta}_{d,i} \\ &- (\hat{J}_{e,i}^T K_{s,i}\hat{J}_{e,i} + K_{\vartheta_i})s_i\end{aligned} \tag{41}$$

where $K_{s,i}$ and K_{ϑ_i} are positive constants.

The estimated dynamic and kinematic parameters $\hat{\theta}_{d,i}$, $\hat{\theta}_{k,i}$ are updated by

$$\dot{\hat{\theta}}_{d,i} = -\Gamma_{d,i}Y_{d,i}^T(\zeta_i,\dot{\zeta}_i,\dot{\zeta}_{r,i},\ddot{\zeta}_{r,i},\beta_i)s_i \tag{42}$$

$$\dot{\hat{\theta}}_{k,i} = -\alpha_i\Gamma_{k,i}Y_{k,i}^T(\zeta_i,\dot{\zeta}_i)K_{o,i}\tilde{x}_{o,i} \tag{43}$$

where $K_{o,i}$ is a positive gain constant, $\Gamma_{d,i}$ and $\Gamma_{k,i}$ are positive definite matrices with opportune dimensions.

The estimated parameters for the internal force regulation are updated by

$$\dot{\hat{\theta}}_{Id,i} = -\Gamma_{Id,i}Y_{Id,i}^T(\zeta_i,F_{Id,i})s_i \tag{44}$$

where $\hat{\theta}_{Id,i}$ is the estimate of $\theta_{Id,i}$ and $\Gamma_{Id,i}$ is a positive definite matrix with opportune dimension.

Remark 9. To avoid employing a separate step to excite the grasped object and estimate its dynamic and kinematic parameters with persistent exiting input signals before manipulation [27], the presented adaptive control in this section provides a more comprehensive approach to concurrently address the kinematic and dynamic uncertainties of both the grasped object and mobile manipulator and no persistent excitation condition is required.

IV. Stability and Convergence Analysis

Two theorems will be given in detail in this section, which together illustrate the stability and error convergence of the proposed distributed adaptive cooperation scheme.

We first define the parameter estimation error as

$$\tilde{\theta}_{\mathrm{sub}} = \hat{\theta}_{\mathrm{sub}} - \theta_{\mathrm{sub}} \tag{45}$$

where the subscript sub denotes the relevant linearized parameters defined above.

To verify the efficacy of the distributed cooperative task allocation (23), we define the first Lyapunov function candidate:

$$\begin{aligned}V_d =& \frac{1}{2}\varepsilon_d^T\varepsilon_d + \frac{1}{2}\kappa_i\sum_{i=1}^N(1-b_i)\mathcal{P}_i\tilde{\theta}_{tr,i}^T\Gamma_{tr,i}^{-1}\tilde{\theta}_{tr,i} \\ =& \underbrace{\frac{1}{2}\varepsilon_{p,d}^T\varepsilon_{p,d} + \frac{1}{2}\kappa_i\sum_{i=1}^N(1-b_i)\mathcal{P}_i\tilde{\theta}_{tr,p,i}^T\Gamma_{tr,i}^{-1}\tilde{\theta}_{tr,p,i}}_{V_{d,p}} \\ &+\underbrace{\frac{1}{2}\varepsilon_{o,d}^T\varepsilon_{o,d} + \frac{1}{2}\kappa_i\sum_{i=1}^N(1-b_i)\mathcal{P}_i\tilde{\theta}_{tr,o,i}^T\Gamma_{tr,i}^{-1}\tilde{\theta}_{tr,o,i}}_{V_{d,o}}\end{aligned} \tag{46}$$

where $\varepsilon_d = [\varepsilon_{d,1}^T,...,\varepsilon_{d,N}^T]^T \in \mathbb{R}^{Nm}$ is the collective error, $\varepsilon_{p,d} = [\varepsilon_{pd,1}^T,...,\varepsilon_{pd,N}^T]^T$ and $\varepsilon_{o,d} = [\varepsilon_{od,1}^T,...,\varepsilon_{od,N}^T]^T$ are both $3N\times 1$ vectors if $m=6$, $\tilde{\theta}_{tr,i} = \hat{\theta}_{tr,i} - \theta_{tr,i}$ is the estimation error of $\theta_{tr,i}$.

The first time derivative of V_d can be expressed as:

$$\dot{V}_d = \varepsilon_d^T\dot{\varepsilon}_d + \kappa_i\sum_{i=1}^N(1-b_i)\mathcal{P}_i\tilde{\theta}_{tr,i}^T\Gamma_{tr,i}^{-1}\dot{\hat{\theta}}_{tr,i} \tag{47}$$

Combining (19) with (20) yields

$$\varepsilon_{d,i} = \delta_i - (1-b_i)\Big[(I_6\otimes\mathcal{F}_{tr}(t))\tilde{\theta}_{tr,i} + \tilde{\mathcal{T}}_{ti}\Big] \tag{48}$$

where $\tilde{\mathcal{T}}_{ti} = \hat{\bar{\mathcal{T}}}_{ti} - \bar{\mathcal{T}}_{ti}$.

Differentiating (19) and considering (23) leads to

$$\dot{\varepsilon}_{d,i} = -\kappa\mathcal{P}_i\gamma_i \tag{49}$$

Incorporating (48), (49), (22) and (24) into (47) gives

$$\begin{aligned}\dot{V}_d =& -\kappa\delta^T\left[\mathcal{P}\left(\mathcal{L}+\mathcal{B}\right)\otimes I_6\right]\delta+\kappa\sum_{i=1}^{N}\mathcal{P}_i(1-b_i)\bar{\rho}_i\\ =& -\frac{\kappa}{2}\delta^T\left[\left(\mathcal{P}\left(\mathcal{L}+\mathcal{B}\right)+\left(\mathcal{L}+\mathcal{B}\right)^T\mathcal{P}\right)\otimes I_6\right]\delta\\ &+\kappa\sum_{i=1}^{N}\mathcal{P}_i(1-b_i)\bar{\rho}_i\\ =& \underbrace{-\frac{\kappa}{2}\delta_p^T\left(\mathcal{Q}\otimes I_3\right)\delta_p+\kappa\sum_{i=1}^{N}\mathcal{P}_i(1-b_i)\bar{\rho}_i}_{\dot{V}_{d,p}}\\ &\underbrace{-\frac{\kappa}{2}\delta_o^T\left(\mathcal{Q}\otimes I_3\right)\delta_o}_{\dot{V}_{d,o}\leq 0}\end{aligned} \tag{50}$$

where $\bar{\rho}_i = \delta_i^T\sum_{j\in\mathcal{N}_i}\tilde{\mathcal{T}}_{ji}+\gamma_i^T\tilde{\mathcal{T}}_{ti}$ and Lemma 1 are employed, $\delta=[\delta_1^T,...,\delta_N^T]^T$ is the concatenation of the estimation error δ_i, $\mathcal{Q}$ is the positive definite matrix defined in Lemma 1. Moreover, $\delta_o=[\delta_{o,1}^T,...,\delta_{o,N}^T]^T\in\mathbb{R}^{3N}$ and $\delta_p=[\delta_{p,1}^T,...,\delta_{p,N}^T]^T\in\mathbb{R}^{3N}$ are two rearranged components of δ.

With (46) and (50), we are ready to give the following theory:

Theorem 1: As for the cooperative task allocation to the mobile manipulators, the proposed distributed estimation law (23) together with the trajectory parameter updating law (24) guarantee the estimation error convergence of the desired allocated task trajectory, i.e., $\delta_i=\hat{\dot{x}}_{d,i}-\mathcal{T}_{ti}-x_{td}\to 0$ and $\dot{\delta}_i\to 0$.

Proof. Please see Appendix B for the proof. ∎

To verify the convergence of the distributed synchronization controller (41), the control law (41) with (29) are incorporated into (40) to establish the following closed-loop dynamic equation as:

$$\begin{aligned}M_{s,i}\dot{s}_i+C_{s,i}s_i =& Y_{d,i}(\zeta_i,\dot{\zeta}_i,\dot{\zeta}_{r,i},\ddot{\zeta}_{r,i},\beta_i)\tilde{\theta}_{d,i}-J_{\phi,i}^TF_{I,i}\\ &+\hat{J}_{\phi,i}^TF_{Id,i}-\left[\hat{J}_{e,i}^T(k_{r,i}+K_{s,i})\hat{J}_{e,i}+K_{\vartheta_i}\right]s_i\end{aligned} \tag{51}$$

Then, the following Lyapunov function candidate $V=\sum_{i=1}^{N}V_i$ is designed:

$$\begin{aligned}V =& \sum\nolimits_{i=1}^{N}\left[\frac{1}{2}s_i^TM_{s,i}s_i+e_i^T\left(1-1/K_\varepsilon\right)K_{s,i}\Lambda_ie_i\right]\\ &+\sum\nolimits_{i=1}^{N}\left(\frac{1}{2}\tilde{\theta}_{Id,i}^T\Gamma_{Id,i}^{-1}\tilde{\theta}_{Id,i}+\frac{1}{2}\tilde{x}_{o,i}^T\alpha_iK_{o,i}\tilde{x}_{o,i}\right)\\ &+\sum\nolimits_{i=1}^{N}\left(\frac{1}{2}\tilde{\theta}_{d,i}^T\Gamma_{d,i}^{-1}\tilde{\theta}_{d,i}+\frac{1}{2}\tilde{\theta}_{k,i}^T\Gamma_{k,i}^{-1}\tilde{\theta}_{k,i}\right)\end{aligned} \tag{52}$$

where K_ε is a positive constant chosen as $K_\varepsilon>1$.

Differentiating V_i with respect to time leads to

$$\begin{aligned}\dot{V}_i =& s_i^T\left[M_{s,i}\dot{s}_i+(\dot{M}_{s,i}s_i)/2\right]+\tilde{x}_{o,i}^T\alpha_iK_{o,i}\dot{\tilde{x}}_{o,i}\\ &+\tilde{\theta}_{d,i}^T\Gamma_{d,i}^{-1}\dot{\tilde{\theta}}_{d,i}+\tilde{\theta}_{Id,i}^T\Gamma_{Id,i}^{-1}\dot{\tilde{\theta}}_{Id,i}+\tilde{\theta}_{k,i}^T\Gamma_{k,i}^{-1}\dot{\tilde{\theta}}_{k,i}\\ &+2e_i^T\left(1-1/K_\varepsilon\right)K_{s,i}\Lambda_i\dot{e}_i\end{aligned} \tag{53}$$

Incorporating (51) into (53) with Property 2 yields

$$\begin{aligned}\dot{V}_i =& s_i^T\left[Y_{d,i}(\zeta_i,\dot{\zeta}_i,\dot{\zeta}_{r,i},\ddot{\zeta}_{r,i},\beta_i)\tilde{\theta}_{d,i}+(\dot{\beta}_iJ_{\phi,i}^TM_oJ_{\phi,i}s_i)/2\right]\\ &-s_i^T\left[\hat{J}_{e,i}^T(K_{s,i}+k_{r,i})\hat{J}_{e,i}+K_{\vartheta_i}\right]s_i+\tilde{x}_{o,i}^T\alpha_iK_{o,i}\dot{\tilde{x}}_{o,i}\\ &+s_i^T(\hat{J}_{\phi,i}^TF_{Id,i}-J_{\phi,i}^TF_{I,i})+2e_i^T\left(1-1/K_\varepsilon\right)K_{s,i}\Lambda_i\dot{e}_i\\ &+\tilde{\theta}_{Id,i}^T\Gamma_{Id,i}^{-1}\dot{\tilde{\theta}}_{Id,i}+\tilde{\theta}_{k,i}^T\Gamma_{k,i}^{-1}\dot{\tilde{\theta}}_{k,i}+\tilde{\theta}_{d,i}^T\Gamma_{d,i}^{-1}\dot{\tilde{\theta}}_{d,i}\end{aligned} \tag{54}$$

in which the term $s_i^T(\hat{J}_{\phi,i}^TF_{Id,i}-J_{\phi,i}^TF_{I,i})$ can be reformulated as:

$$s_i^T\left(\hat{J}_{\phi,i}^TF_{Id,i}-J_{\phi,i}^TF_{I,i}\right)=s_i^TJ_{\phi,i}^T\tilde{F}_{I,i}+s_i^TY_{Id,i}\tilde{\theta}_{Id,i} \tag{55}$$

where $\tilde{F}_{I,i}=F_{Id,i}-F_{I,i}$ is the internal force error.

Folding (32), (39) and the updating laws (42)-(44) into (54) gives

$$\begin{aligned}\dot{V}_i \leq& -\left(1-\frac{1}{K_\varepsilon}\right)S_{x,i}^TK_{s,i}S_{x,i}+2e_i^T\left(1-\frac{1}{K_\varepsilon}\right)K_{s,i}\Lambda_i\dot{e}_i\\ &-\alpha_i^2\left(K_{s,i}+K_{o,i}-K_\varepsilon K_{s,i}\right)\tilde{x}_{o,i}^T\tilde{x}_{o,i}-k_{r,i}\left\|\hat{J}_{e,i}s_i\right\|^2\\ &+s_i^TJ_{\phi,i}^T\tilde{F}_{I,i}-s_i^T\left(K_{\vartheta_i}-\vartheta_i\right)s_i\end{aligned} \tag{56}$$

whose derivation detail is attached in Appendix C and the following inequality is used

$$-2\alpha_iK_{s,i}S_{x,i}^T\tilde{x}_{o,i}\leq\frac{1}{K_\varepsilon}S_{x,i}^TK_{s,i}S_{x,i}+\alpha_i^2K_\varepsilon K_{s,i}\tilde{x}_{o,i}^T\tilde{x}_{o,i} \tag{57}$$

The last but one term on the right side of (56) satisfies:

$$\begin{aligned}s_i^TJ_{\phi,i}^T\tilde{F}_{I,i} =& (T_{A,i}J_{e,i}s_i)^T\left(J_{o,i}^\dagger\right)^T\tilde{F}_{I,i}\\ \leq& \left\|T_{A,i}J_{e,i}s_i\right\|\left(\left\|\bar{F}_{Id,i}\right\|+\left\|\bar{F}_{s,i}\right\|\right)\end{aligned} \tag{58}$$

where the following inequality is employed

$$\begin{aligned}\left\|\left(J_{o,i}^\dagger\right)^T\tilde{F}_{I,i}\right\| =& \left\|\left(J_{o,i}^\dagger\right)^T\left(F_{Id,i}-F_{I,i}\right)\right\|\\ =& \left\|\bar{F}_{Id,i}-\bar{F}_{I,i}\right\|\\ \leq& \left\|\bar{F}_{Id,i}\right\|+\left\|\bar{F}_{s,i}\right\|\end{aligned} \tag{59}$$

Considering (34) and (58), (56) can be further simplified to

$$\begin{aligned}\dot{V}_i \leq& -\alpha_i^2\left(K_{s,i}+K_{o,i}-K_\varepsilon K_{s,i}\right)\tilde{x}_{o,i}^T\tilde{x}_{o,i}-s_i^T\left(K_{\vartheta_i}-\vartheta_i\right)s_i\\ &-\left(1-\frac{1}{K_\varepsilon}\right)K_{s,i}\left(\dot{e}_i^T\dot{e}_i+e_i^T\Lambda_i^T\Lambda_ie_i\right)\\ \leq& 0\end{aligned} \tag{60}$$

where the positive constants K_{ϑ_i}, K_ε, $K_{o,i}$, $k_{r,i}$ are set as

$$\begin{cases}K_{\vartheta_i}>\vartheta_i\\ K_\varepsilon>1\\ K_{o,i}>\left(K_\varepsilon-1\right)K_{s,i}\\ k_{r,i}\geq\left\|T_{A,i}J_{e,i}s_i\right\|\left(\left\|\bar{F}_{Id,i}\right\|+\left\|\bar{F}_{s,i}\right\|\right)/\left\|\hat{J}_{e,i}s_i\right\|^2\end{cases} \tag{61}$$

Now we are in position to formulate the following theorem.

Theorem 2: For N uncertain mobile manipulators interacting on the graph satisfying Assumption 3 and cooperatively grasping an unknown object, the distributed adaptive control law (41) with parameter updating laws (42)-(44) can guarantee the stability of the robotic ensemble and lead to the motion synchronization and the convergence of Cartesian-space motion tracking errors, i.e., $\Delta x_{e,i}, \Delta \dot{x}_{e,i} \to 0$, $\Delta x_{e,i} - \Delta x_{e,j} \to 0$ and $\Delta \dot{x}_{e,i} - \Delta \dot{x}_{e,j} \to 0$ as $t \to \infty$, $\forall i \in \{1, 2, ..., N\}$. Furthermore, the internal force tracking error approaches to the neighborhood of the zero point.

Proof. Please see Appendix C for the proof. ■

V. Simulations

In this section, we present the simulation results to confirm the efficacy of the proposed distributed cooperation scheme. Four nonholonomic mobile manipulators are involved and their motions are constrained in the horizontal X-Y plane. The communication topology among the four networked mobile manipulators is shown in Fig. 3. Dynamic and kinematic parameters of the mobile manipulator are listed in Table II. Three cases are studied to demonstrate the interaction between the complex interconnected mechanism, the distributed manner and the synchronization considered in this work. These simulations are implemented by employing Simulink and SimMechanics 2G. Nonholonomic constraints imposed on the mobile platform are simulated based on the Lagrange Equation and Lagrange multiplier method. In Case B and Case C, the mobile manipulators only exchange the estimated cooperative task position $\hat{\bar{x}}_{d,i}$ and the observed Cartesian-space position $x_{o,i}$ with their neighbors, as implied by the mathematical expression of the proposed scheme. The desired trajectory of the virtual leader is supposed to be known only to Robot 1 (Please see Fig. 3 for the robot number). Then the Laplacian matrix $\mathcal{L}$ and the matrix $\mathcal{B}$ can be computed based on the topology shown in Fig. 3. The vector w defined in Lemma 1 associated with the communication graph is $w = [1, 3, 4, 2]^T$. The initial position derivation of the EE of Robot 1 $r_{o1} = [0, -1, 0]^T$ and the relative position between the EEs of the mobile manipulators are set as $r_{12} = [-2, 0, 0]^T$, $r_{13} = [-2, 2, 0]^T$ and $r_{14} = [0, 2, 0]^T$.

TABLE II
PHYSICAL PARAMETERS OF THE MOBILE MANIPULATOR AND THE GRASPED OBJECT

Part	Body	m_i (kg)	I_i (kg·m^2)	l_i (m)	l_{ci} (m)
Manipulator	Link1	6.5	0.12	0.4	0.28
	Link2	5.0	0.42	0.285	0.20
	Link3	2.6	0.10	0.35	0.25
Mobile base	Mass		Moments of Inertia		COM
	10 (kg)		diag([0, 0, 1]) (kg·m^2)		Geometric center
	Wheel Radius		Wheelbase		Rear Track
	0.15 (m)		0.5 (m)		0.5 (m)
Object	Mass		Moments of Inertia		COM
	6 (kg)		diag([0, 0, 8]) (kg·m^2)		Midpoint of EE1-EE4

A. Interaction of the interconnected system

This case study presents the results under two different desired load distribution schemes, which aims at validating the feasibility of the distributed dynamic model of the whole interconnected system as given in (13) and showing the nature of wrench synthesis/decomposition without other potentially disturbances. To highlight the relation between resultant interaction forces and designated load distribution in (12), the system dynamics and kinematics here are assumed to be certain and the cooperative task is exactly allocated to each mobile manipulator. The desired cooperative trajectory is selected as

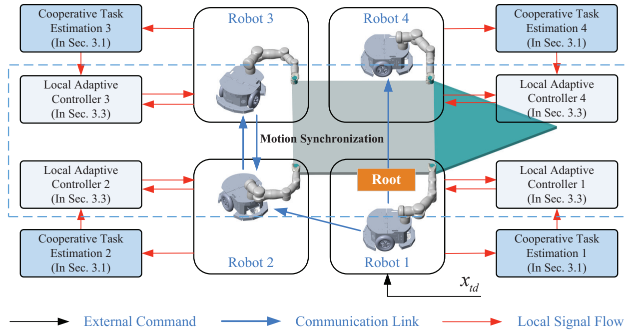

Fig. 3: Communication topology of the networked mobile manipulators

$$x_{td} = \begin{bmatrix} 1.04(\sqrt{3}+1) + t^3/25 + t^2/5 \\ -t^3/50 + 3t^2/10 \\ -\pi t^3/3000 + \pi t^2/200 \end{bmatrix}$$

Fig. 4 presents the actual load sharing $\beta_{r,i}$ during the cooperative transport under two different load distribution schemes, i.e., Case A-1: $\beta_1 = \beta_4 = 0I_3$, $\beta_2 = 0.8I_3$, $\beta_3 = 0.2I_3$ and Case A-2: $\beta_1 = 0.35I_3$, $\beta_2 = 0.3I_3$, $\beta_3 = 0.2I_3$, $\beta_4 = 0.15I_3$. Here $\beta_{r,i}$ is computed based on the physically plausible wrench decomposition method proposed in [40]. From this figure, one can note that after the interconnected system achieves controlled dynamic balance, approximately after $t = 1$ s, the actual load sharing parameters $\beta_{r,i}$ match quite well with the desired load distribution parameters β_i, which implies the applicability of the distributed dynamics.

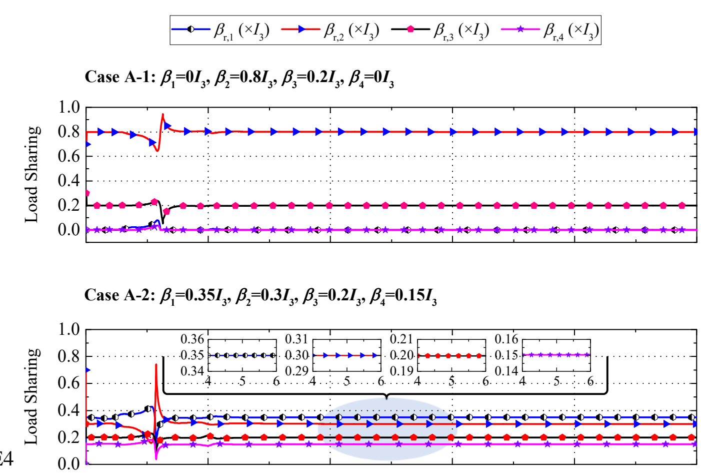

Fig. 4: Actual load sharing under two different load distribution schemes

B. Distributed kinematic cooperation

In this case, four networked nonholonomic mobile manipulators are controlled in a distributed way and

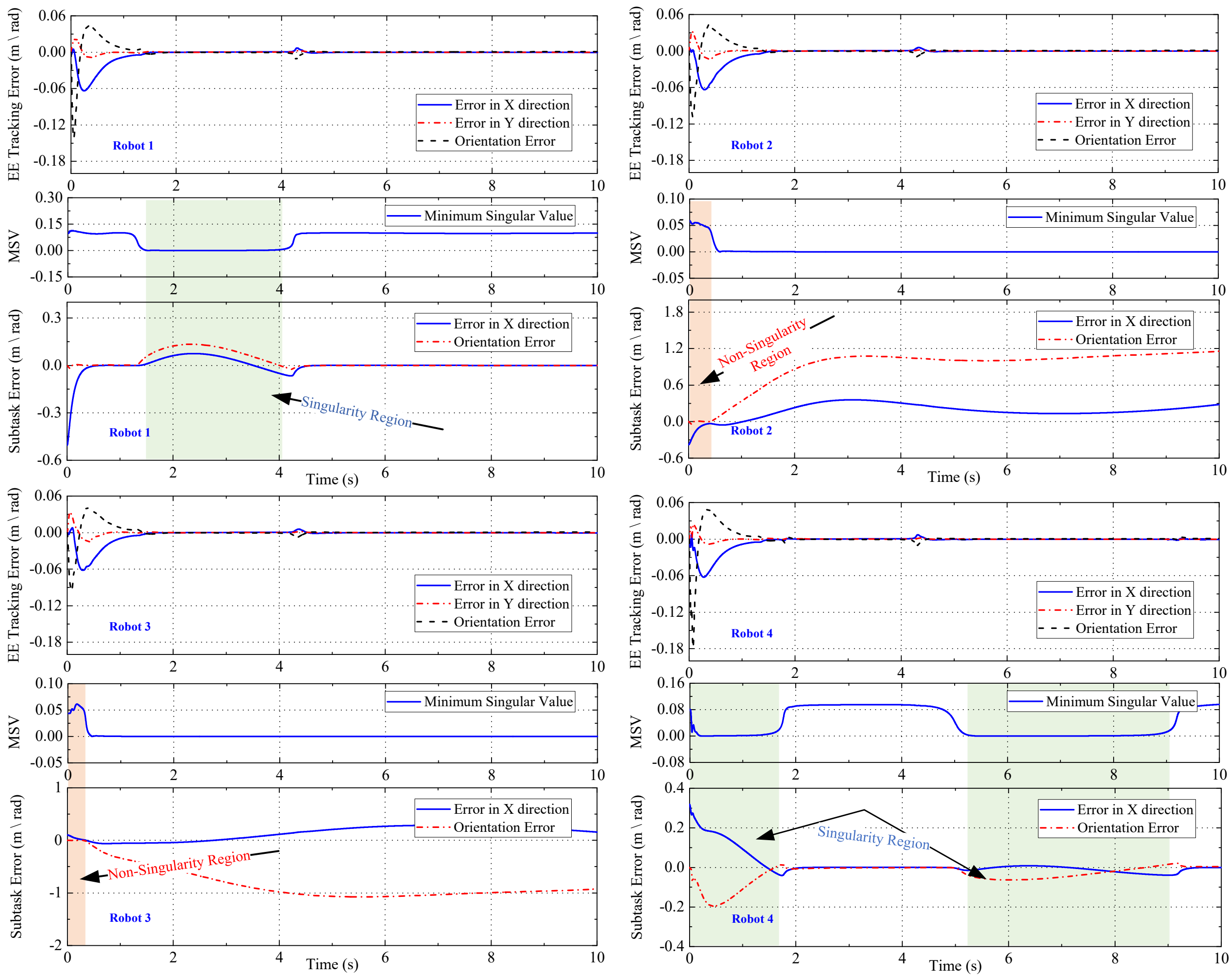

Fig. 5: Primary task and subtask tracking errors of the four nonholonomic mobile manipulators

their end-effector motions are coordinated so that the equivalent centroid of the kinematic cooperation task (ECCT, denoted by $x_{\text{ecct}} = [x_{\text{ec}}, y_{\text{ec}}, \alpha_{\text{ec}}]^T \in \mathbb{R}^3$ and visualized by blue triangle in the supplementary video) can track the desired trajectory of the virtual leader (DTVL, denoted by $x_{\text{dtvl}} \in \mathbb{R}^3$ and visualized by the red triangle in the supplementary video). Inspired by the definition of the centroid variable in [31] and to maintain the consistency between Case B and Case C, the definition of x_{ecct} is given as $x_{\text{ecct}} = \sum_{i=1}^{4} x_{e,i}/4 + [(R(\alpha_{\text{ec}})r_{\text{ec}})^T, 0]^T$, where $R(\alpha_{\text{ec}}) = [\cos(\alpha_{\text{ec}}), -\sin(\alpha_{\text{ec}}); \sin(\alpha_{\text{ec}}), \cos(\alpha_{\text{ec}})]$ denotes the rotation matrix associated with the rotation angle of ECCT and $r_{\text{ec}} = [1.04 \times (\sqrt{3}+1), 0]^T$ denotes the virtual link between ECCT and the kinematic centroid of the four end-effector frames. The DTVL is chosen as

$$x_{\text{dtvl}} = \begin{bmatrix} 1.04(\sqrt{3}+1) + 0.1 + 3t^2/20 - t^3/100 \\ 0.1 + 0.3\sin(0.1\pi t) + 0.1\cos(0.1\pi t) \\ \quad +0.3\sin(0.2\pi t) - 0.1\cos(0.2\pi t) \\ \pi/15 - \pi t^2/500 + \pi t^3/7500 \end{bmatrix}$$

which can be linearized according to (17). The allocated task of this cooperative task to each robot agent is taken as the primary task. The local subtask for each nonholonomic mobile manipulator $x_{sd,i} = [x_{M,i}, \varphi_{M,i}]^T$ is set as

$$x_{sd,i} = \begin{bmatrix} 0.1 + 3t^2/20 - t^3/100 \\ \pi t^2/25 - 2\pi t^3/375 \underbrace{\mp\pi/3}_{fori=2,3} \end{bmatrix}$$

where $\varphi_{M,i}$ and $x_{M,i}$ denote the orientation and the addition to the initial x-coordinate of the mobile base.

The internal wrench regulation (29) and the object dynamics in the synthesized dynamic equation (13) are set to null. The dynamic regressor $Y_{d,i}(\zeta_i, \dot{\zeta}_i, \ddot{\zeta}_i, 0)$ is a 5×74 matrix and the kinematic regressor $Y_{k,i}(\zeta_i, \dot{\zeta}_i)$ is a 3×9 matrix, whose analytical expressions are not presented here. Fig. 5 shows the minimum singular value of the projected Jacobian and the tracking results of the primary task and subtask for each robot, from which one can conclude that the local subtask tracking performance is partly sacrificed to maintain the high tracking performance of the primary task when the projected Jacobian is singular. In non-singularity regions, both of the tasks are fully executed. It should be noted that the singularity-robust technique (36) may introduce a sudden change of the joint-space reference velocity $\dot{\zeta}_{r,i}$ during the transition phase

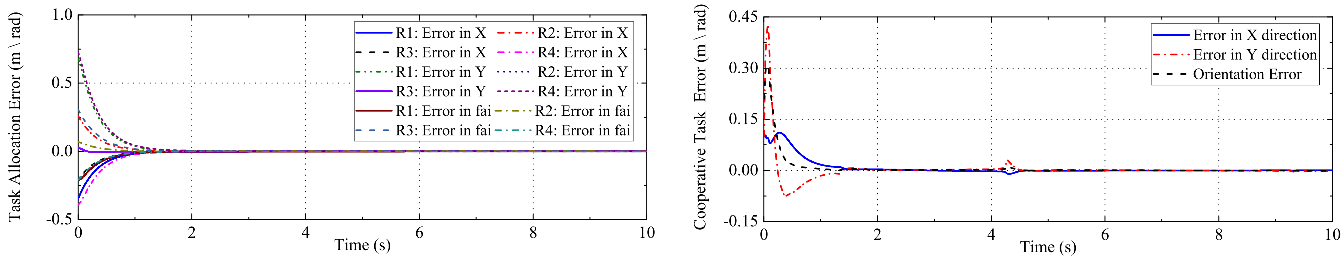

(a) (b)

Fig. 6: (a) Task allocation error and (b) cooperative task tracking error in the distributed kinematic cooperation task

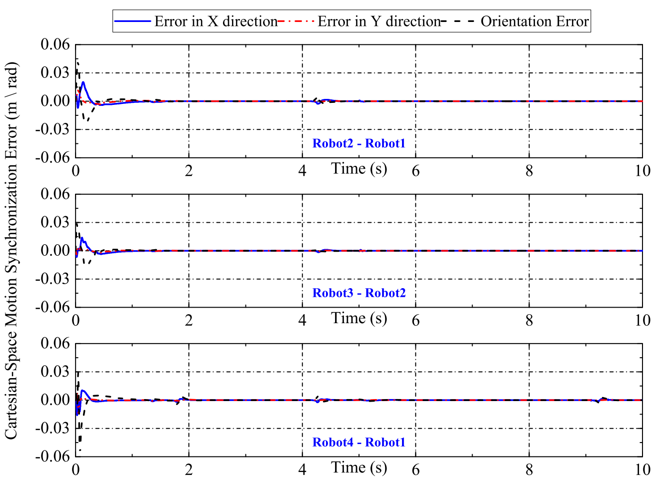

Fig. 7: Synchronization errors between the four mobile manipulators

between singularity and non-singularity, which further leads to a transient impact on the input torques. This acts as the primary cause of the slight performance degradation at about $t = 4$ s. This phenomenon can be alleviated by adjusting the singularity region parameter Δ_i and the maximum of the damping factor $\lambda_{\max,i}$ defined in (36). In practical implementation, we have to strike a balance between the singularity robustness and the tracking performance.

The convergence of the synchronization errors between the Cartesian-space motions of the mobile manipulators illustrated in Fig. 7 and the convergence of the distributed task allocation error shown in Fig. 6 (a) together contribute to the convergence of the cooperative task tracking error presented in Fig. 6 (b), as expected by Theorem 2.

C. Distributed cooperative transport

In this case, the desired internal wrench is set to zero due to the tight connection condition. To show the superiority of the proposed distributed adaptive control scheme (DA scheme) in the cooperative task tracking and internal wrench regulation, a conventional visual servoing control scheme (NA scheme) without adaptation is introduced. These two comparative schemes share the same control gains, initial values and communication topology and both have access to the pose feedback signals. The desired trajectory for the operational point of the grasped object is given as $x_{td} = [1.04(\sqrt{3}+1) + t^3/25 + t^2/5, -t^3/50 + 3t^2/10, 0]^T$. Dynamic parameters of the grasped object and kinematic parameters associated with the grasp matrix are unknown to the robotic agent. The task allocation parameters and most of the control gains are selected as in Case B, while $\varepsilon_i = 5$, Δ_i=0.08 and $\lambda_{\max,i}$= 0.15. The desired load distribution to each nonholonomic mobile manipulator is set as: $\beta_1 = 0.5I_3$, $\beta_2 = 0.5I_3$ and $\beta_3 = \beta_4 = 0_{3\times3}$. Tracking errors of the operational point in this cooperative transport task are presented in Fig. 8. Maximum and root mean square (RMS) of the 2-norm of the tracking error are listed in Table III, which implies that the proposed distributed adaptive cooperation scheme significantly improves the tracking performance in the cooperative transport task even in the presence of dynamic/kinematic uncertainties and constrained communication.

TABLE III
PERFORMANCE INDEXES WITH TWO COMPARATIVE SCHEMES

	Proposed adaptive scheme		Non-adaptive scheme	
	Max	RMS	Max	RMS
Δx_t	0.0074	0.003	0.2448	0.115
$F_{e,1}$	24.59	11.2	200.9	100.7
$F_{e,2}$	27.75	13.13	135.5	56.5
$F_{e,3}$	17.98	4.61	222.1	105.1
$F_{e,4}$	30.70	7.92	133.4	55.7

In addition, Fig. 9 displays the measured interaction forces between the EEs of the mobile manipulators and the grasped object during task execution with two schemes, from which one can easily conclude that the proposed adaptive scheme enjoys much smaller interaction forces than the conventional NA scheme. According to the constraints defined in (25), smaller interaction force implies smaller internal force and better transient performance. This advantage results from the synchronization of the allocated tasks achieved by the distributed cooperative task allocation in Section 3.1 and the motion synchronization achieved by the distributed adaptive control in Section 3.3.

In practical implementation, requirement of EE force/torque sensors can be avoided at the expense of a small performance degradation. Using the Cauchy-Schwartz inequality and considering $\|T_{A,i}J_{e,i}s_i\| = \|T_{A,i}Y_{k,i}(\zeta_i, s_i)\theta_{k,i}\|$, the last inequality in (61) can be reformulated as $k_{r,i} \geq k_{rc}||T_{A,i}Y_{k,i}(\zeta_i, s_i)||_2/||\hat{J}_{e,i}s_i||^2$ where k_{rc} is a positive constant and $\|\bullet\|_2$ is the Frobenius norm. In addition, a common practice in robust control is further adopted

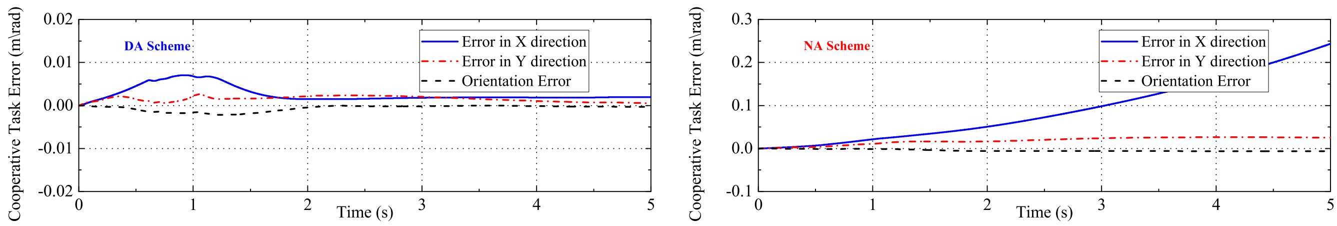

Fig. 8: Cooperative transport error with two comparative schemes: The left subfigure shows the tracking error with proposed distributed adaptive (DA) scheme; The right subfigure demonstrates the tracking error with conventional non-adaptive (NA) scheme

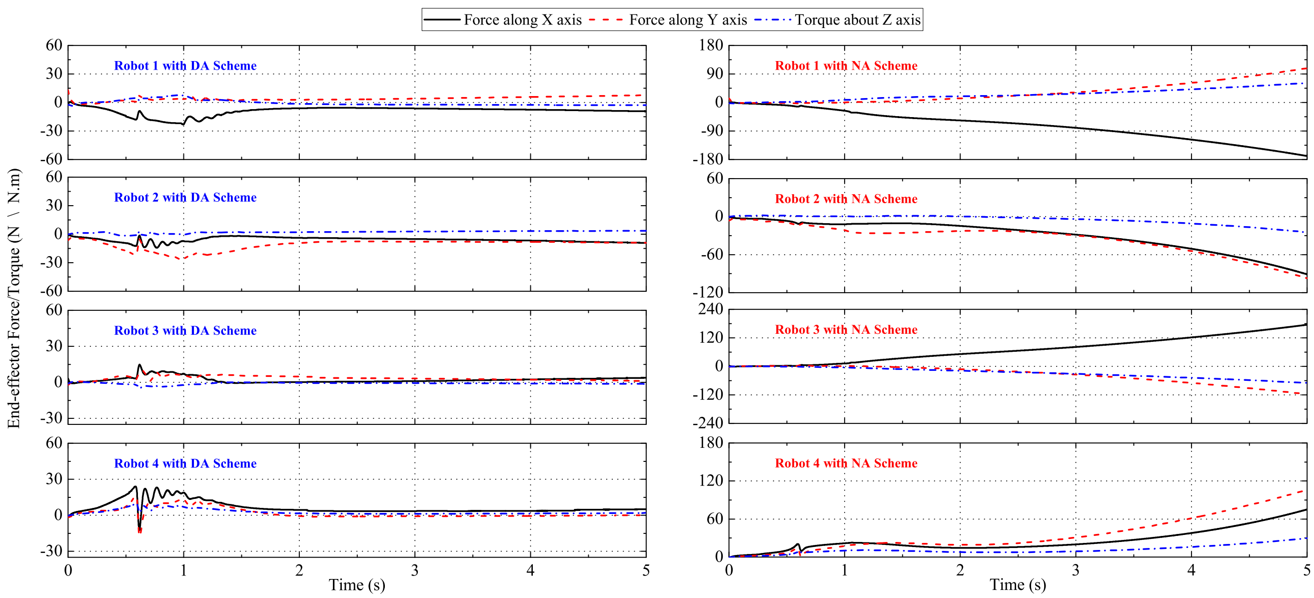

Fig. 9: Interaction forces of the four mobile manipulators with two comparative schemes: The left part shows the interaction forces with proposed distributed adaptive (DA) scheme; The right part demonstrates the interaction forces with conventional non-adaptive (NA) scheme

to guarantee the boundedness of $k_{r,i}$, i.e., $k_{r,i} \geq k_{rc}||T_{A,i}Y_{k,i}(\zeta_i, s_i)||_2/||\hat{J}_{e,i}s_i||^2$ if $||\hat{J}_{e,i}s_i||^2 \geq \mu$ and $k_{r,i} = k_{rc}||T_{A,i}Y_{k,i}(\zeta_i, s_i)||_2/\mu$ if $||\hat{J}_{e,i}s_i||^2 < \mu$, where μ is a positive constant. Another advantage of this reformulation is that the stability of the system can be more easily guaranteed because the unavoidable lag due to the mechanical causality of the force/torque signal feedback can be avoided.

Different from the results in other related papers that the internal force is presented to be very large in the presence of small kinematic discrepancy, here we employ very small control gains in the simulations to highlight the improvement of tracking performance with the proposed adaptive scheme. The advantage of this proposed scheme in terms of tracking performance will be more competitive compared to its non-adaptive counterpart when the velocity of the desired trajectory changes more sharply or the dynamic uncertainties are more severe. It should be noted that potential communication delay in the network may degrade the control performance or even result in system instability, especially for the tight cooperation task considered here. A queuing/buffering method, as a simple but effective delay compensation technique, can be adopted in practice when the hard-real-time task execution is not required [53].

VI. Hardware Experiment

The main focus of the conducted experiment is to corroborate theoretical findings regarding the distributed cooperation. A video of a 3-D cooperative manipulation task is available in the supplementary material.

A. Experimental setup

The experimental setup and the communication network are illustrated in Fig. 10. Three mobile manipulators are involved in this experiment. The whole control architecture is implemented based on Robot Operating System (ROS) with which the issues of task schedule/synchronization and distributed communication networks in multi-robot systems are greatly simplified. A remote workstation for this cooperation task is set up only for system initializing and state monitoring. Each mobile manipulator comprises a 7-DOF Franka Emika Panda manipulator and a custom holonomic mobile platform. An Intel NUC computer (Intel i7-8559U CPU with 8 cores and 16 GB RAM) is equipped as a local workstation. Due to our hardware architecture, the manipulator and the mobile platform are controlled in different ways, i.e., torque-based control for the manipulator and velocity-based control for the mobile platform. Trajectory planning for manipulator and platform are integrated and executed on a higher level in the local workstation to guarantee their motion coordination. The local controller/planning and coordination algorithms are running in a loop at 1 kHz and the commanded joint torques/platform velocity are respectively sent to the control box of the manipulator and the Arduino board for the mobile platform. Soft real-time execution is guaranteed by the PREEMPT_RT kernel installed in the local workstation. The local workstation communicates with the control box based on User Datagram Protocol (UDP) and with the Arduino based on RS232 serial communication protocol, which together contribute to 1 kHz data transmission rate. In the experiment, a Qualisys Motion Capture System consisting of multiple industrial grade tracking cameras is employed to provide accurate localization signals and real-time pose feedback of the end-effectors at the rate of 300 Hz. This is achieved by attaching two groups of optical markers to the body of each mobile manipulator, one group for the mobile platform and the other group for the end-effector. Also, a marker group is allocated to each grasp handle, which facilitates the target recognition and helps the robots locate the respective reference grasp point on the object.

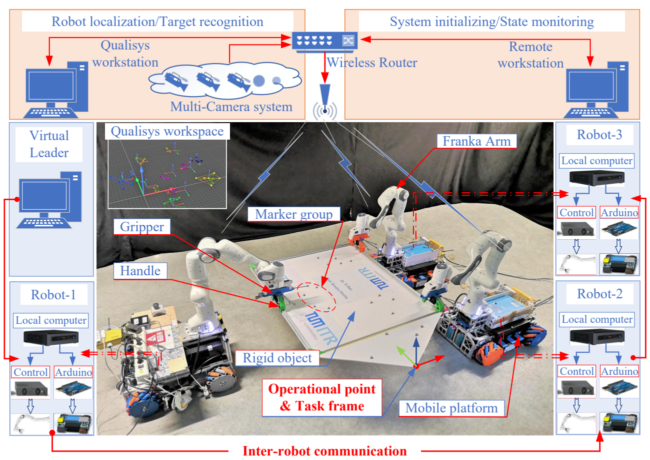

Fig. 10: Experimental setup and communication network of the multiple mobile manipulator system

A ROS node running on a separate PC is designed to act as the virtual leader of the multi-robot system and generates online the desired trajectory for the operational point of the grasped object. The robots communicate with their neighbours according to the inter-robot communication topology shown in Fig. 10 (highlighted by the red arrow-shaped line). In this experiment, the inter-robot communication is based on a wired network to enable reliable data transfer. For the implementation of wireless communication, the readers are suggested to use RT wireless protocol to minimize the communication delay and improve the transmission frequency. The state-of-the-art RT wireless protocol can provide sufficiently high sampling rate up to 6 kHz [54]. This is fast enough to support high-speed control systems which typically require 1 kHz or higher sampling rate and the guaranteed upper bound of delay is less than 1 ms.

In the experiment, the friction between the gripper and the object in the manipulation phase is sufficient to guarantee the rigid grasp. Thus the multi-arm grasp type is applicable here and the friction term in the grasp model is then hidden behind the dynamic equation of the mobile manipulators. In addition, it is worth mentioning that the mass of the object in this experiment is about 4 kg, which is beyond the 3 kg load capacity of each individual manipulator. Considering that the validity of the proposed scheme when addressing dynamic uncertainties has been checked in the Simulation in detail and the uncertain gravity of the grasped object predominates in the performance degradation when regular-speed manipulation task is considered, the proposed adaptive control scheme in this experiment will mainly focus on the uncertain gravity in the system dynamics. This help us to efficiently validate the proposed scheme without loss of generality since the gravitational term and other higher-order terms are equivalent in terms of system dynamics.

B. Experimental results

In this experiment, the three mobile manipulators tightly grasp and manipulate a rigid object so that the cooperative task frame, whose origin coincides with the operational point (shown in Fig. 10), can track a piecewise trajectory specified by the virtual leader. Motion of this frame is recorded by the Qualisys system. Robot 1, as the root of the communication network, has access to the desired trajectory of the task frame and the virtual leader can be viewed as its neighbor. Robot 2, whose estimated local trajectory is subscribed by Robot 3, receives the estimated local trajectory of Robot 1 in real-time. Before the manipulation task starts, the three robotic agents autonomously approach to the neighborhood of the object and grasp the object by using the pose information of the handles. Once the object is tightly grasped, the rigid formation relationship among the end-effectors of the three robots is established. Then each robot reads once its neighbours' poses and calculates the relative displacement/orientation with respect to its local frame, i.e., ${}^{i}r_{ji}$ and $\bar{R}_{i,i}$.

The parameters for the task allocation in this experiment are chosen as $\kappa = 2$ and $\Gamma_{tr,i} = 20$. The constant matrix $\mathcal{P}$ defined in Lemma 1 is $\mathcal{P} = \mathrm{diag}(1, 1/2, 1/3)$, which is computed according to the network topology presented in Fig. 10. The control gains are set to be $K_{s,i} = 15$, $K_{\vartheta_i} = 10$ and $\Lambda_i = \mathrm{diag}(20I_3, 1.5I_3)$, which are much smaller than those of the conventional high-stiffness controllers. High manipulation performance is then maintained by the employed dynamic compensation term $Y_{d,i}\hat{\theta}_{d,i}$. In this way, the interconnected robotic system is tolerant of relatively large tracking errors during the transient phase and therefore is much safer. The observer gain is set to be $\alpha_i = 20$ and the adaptive gains are given by $K_{o,i} = 30$, $\Gamma_{k,i} = 5I_6$, $\Gamma_{d,i} = 0.001I_3$ and $\Gamma_{Id,i} = 0.005I_3$. The desired trajectory for the task frame and its actual trajectory measured by Qualisys in the 3-D manipulation phase are both shown in Fig. 11. Together with the root mean square of the tracking errors listed in Table IV, it can be observed that the cooperative task tracking accuracy is still ensured, especially considering the small control gains, the uncertainties and the distributed communication architecture. In this experimental setup, no force/torque sensor is equipped. By means of the interfaces to the manipulator dynamics and

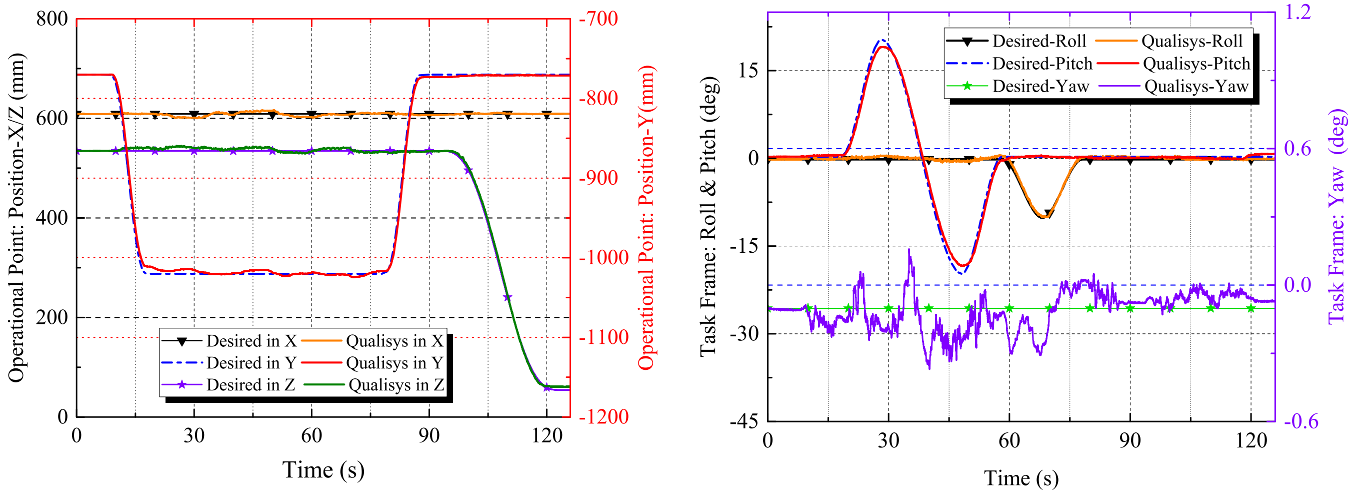

Fig. 11: Operational trajectory tracking results of the task frame (operational point) in 3-D manipulation task: The left subfigure is a double Y-axis graph and shows the position tracking results of the operational point with respect to the world frame. The three solid lines represent the position acquired by the Qualisys system (yellow for X, red for Y and olive for Z) and the three lines with symbols (or dash-dotted line) are the desired trajectories specified by the virtual leader. Tracking results in X and Z direction are graphed by the left Y axis and the right Y axis is used to graph the results in Y direction (red solid line and blue dash-dotted line); The right subfigure shows the time history of the task frame orientation also with two Y axes. The three solid lines represent the actual orientation of the task frame (yellow for roll angle, red for pitch angle and purple for yaw angle) and the three lines with symbols (or dash-dotted line) represent the profiles of the desired orientation. Tracking results of the roll and pitch angles are graphed by the left Y axis and the right Y axis is used to graph the results of the yaw angle (purple solid line and green dash-dotted line)

the join torque information provided by Franka [55], the interaction wrenches between the end-effectors and the grasped object are estimated based on the momentum observer [56]. Profiles of the interaction wrenches are presented in Fig. 12, from which one can conclude that the internal wrench, as a component of the interaction wrench, is bounded.

TABLE IV
ROOT MEAN SQUARE OF THE TRACKING ERROR

X (mm)	Y (mm)	Z (mm)	Roll (deg)	Pitch (deg)	Yaw (deg)
3.027	3.813	4.694	0.301	0.571	0.084

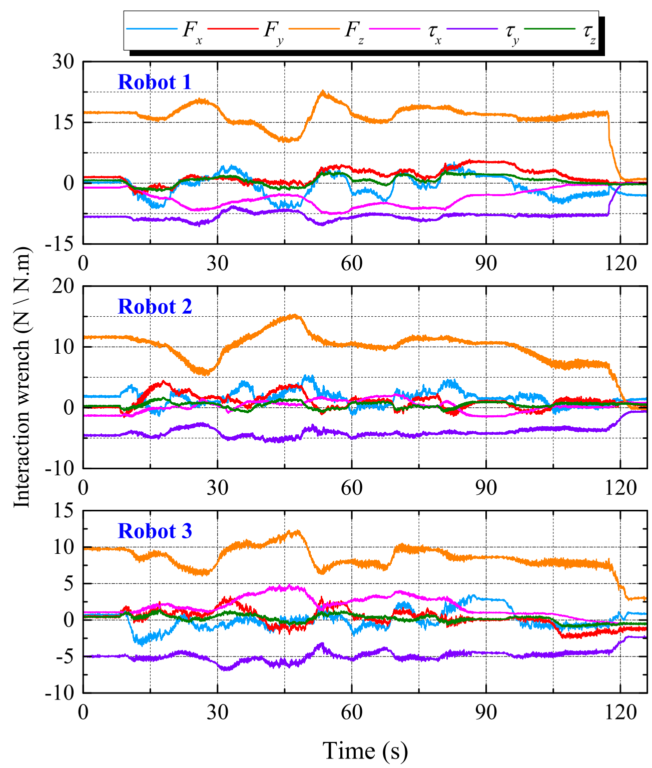

Fig. 12: Interaction wrenches between the object and the end-effectors. After $t >= 120$ s, the three mobile manipulators lay down and release the grasped object, all the interaction wrenches approximate to zeros.

VII. Conclusion

This paper presents a fully distributed cooperation scheme for networked mobile manipulators. In the first phase of the scheme pipeline, an adaptation-based estimation law is established for each mobile manipulator to estimate the linearized desired trajectory of the virtual leader in a distributed way. Pose formation idea is incorporated here to achieve cooperative task allocation considering the offset between the task frame and end-effector frame of the robotic agents. Then based on the existing works, physical constraints imposed on the desired load distribution and desired internal force are proposed in terms of wrench synthesis, which lays a foundation for tight cooperation problem. In the last phase, a set of distributed adaptive controllers is proposed to achieve synchronization between end-effector motions of the networked mobile manipulators irrespective of the kinematic and dynamic uncertainties in both the mobile manipulators and the tightly grasped object. This controlled synchronization contributes to the improvement of the cooperative task tracking performance and the transient performance quantified by the 2-norm of the interaction/internal forces. In addition, redundancy of each robotic agent is locally resolved on the velocity level and is utilized to achieve subtasks based on a multi-priority strategy. Noisy Cartesian-space velocities are avoided here. This complete scheme is independent from the object's center of mass by employing a task-oriented strategy and formation-based cooperative control and does not require any persistent excitation condition to achieve the tracking objectives. It is theoretically proven that convergence of the task tracking error and synchronization error are guaranteed. Simulation results of two typical cooperation tasks, i.e., kinematic cooperation and dynamic cooperation, are both illustrated to validate the efficacy and demonstrate the expected performance of the proposed scheme. Finally, a 3-D manipulation experiment conducted with three mobile manipulators confirms the applicability of the presented results in the distributed cooperation task.

ACKNOWLEDGMENT

The authors would like to express their appreciation to the anonymous reviewers for their helpful and constructive comments. They also would like to thank Dr. Hanlei Wang for his great help and insightful suggestions in this work.

APPENDIX

A. Proof of Property 2

Proof.

$$M_{r,i} = \begin{bmatrix} H_{v,i}^T M_{v,i} H_{v,i} & H_{v,i}^T M_{vm,i} \\ M_{mv,i} H_{v,i} & M_{m,i} \end{bmatrix}$$

$$B_{r,i}(q_i) = \begin{bmatrix} H_{v,i}^T B_{v,i} & 0 \\ 0 & B_{m,i} \end{bmatrix}$$

$$C_{r,i} = \begin{bmatrix} H_{v,i}^T C_{v,i} H_{v,i} + H_{v,i}^T M_{v,i} \dot{H}_{v,i} & H_{v,i}^T C_{vm,i} \\ M_{v,i} \dot{H}_{v,i} + C_{mv,i} H_{v,i} & C_{m,i} \end{bmatrix}$$

$$G_{r,i} = [G_{v,i}^T H_{v,i}, G_{m,i}^T]^T$$

Then, we have

$$\begin{aligned} \dot{M}_{r,i} - 2C_{r,i} &= \frac{d \begin{bmatrix} H_{v,i}^T M_{v,i} H_{v,i} & H_{v,i}^T M_{vm,i} \\ M_{mv,i} H_{v,i} & M_{m,i} \end{bmatrix}}{dt} \\ &- 2 \begin{bmatrix} H_{v,i}^T C_{v,i} H_{v,i} + H_{v,i}^T M_{v,i} \dot{H}_{v,i} & H_{v,i}^T C_{vm,i} \\ M_{v,i} \dot{H}_{v,i} + C_{mv,i} H_{v,i} & C_{m,i} \end{bmatrix} \\ &= \begin{bmatrix} H_{v,i} & 0 \\ 0 & I \end{bmatrix}^T [\dot{M}_i(q_i) - 2C_i(q_i, \dot{q}_i)] \begin{bmatrix} H_{v,i} & 0 \\ 0 & I \end{bmatrix} \end{aligned} \tag{A1}$$

Considering the definition of the synthesized inertia matrix $M_{s,i}$ and Coriolis/Centrifugal matrix $C_{s,i}$ given in (13)

$$\begin{aligned} &\dot{M}_{s,i} - 2C_{s,i} - \dot{\beta}_i J_{\phi,i}^T M_o J_{\phi,i} \\ =&\dot{M}_{r,i} + \dot{\beta}_i(t) J_{\phi,i}^T M_o J_{\phi,i} + \beta_i(t) \frac{dJ_{\phi,i}^T M_o J_{\phi,i}}{dt} \\ &- 2(C_{r,i} + \beta_i(t)[J_{\phi,i}^T C_o J_{\phi,i} + J_{\phi,i}^T M_o \frac{dJ_{\phi,i}}{dt}]) \\ &- \dot{\beta}_i J_{\phi,i}^T M_o J_{\phi,i} \\ =&(\dot{M}_{r,i} - 2C_{r,i}) + \beta_i(t) J_{\phi,i}^T (\dot{M}_o - 2C_o) J_{\phi,i} \\ =&\begin{bmatrix} H_{v,i} & 0 \\ 0 & I \end{bmatrix}^T [\dot{M}_i(q_i) - 2C_i(q_i, \dot{q}_i)] \begin{bmatrix} H_{v,i} & 0 \\ 0 & I \end{bmatrix} \\ &+ \beta_i(t) J_{\phi,i}^T (\dot{M}_o - 2C_o) J_{\phi,i} \end{aligned} \tag{A2}$$

According to the property of the dynamics of mechanical system, one can know that $(\dot{M}_i - 2C_i)$ and $(\dot{M}_o - 2C_o)$ are skew-symmetric matrices by particular choice of C_i and C_o. Therefore, the skew-symmetric property of $\dot{M}_{s,i} - 2C_{s,i} - \dot{\beta}_i J_{\phi,i}^T M_o J_{\phi,i}$ is proven. ∎

B. Proof of Theorem 1

Proof. Before establishing the stability analysis, we would like to introduce a corollary and a lemma first. Based on the passive decomposition approach [57] and input-output property [58], the following corollary can be concluded:

Corollary A-1. Define $x = [x_1, x_2 ... x_n]^T$ and $y = [y_1, y_2 ... y_n]^T$. For the first-order dynamics $\dot{x} = -\mathcal{L}x + y$ where $\mathcal{L}$ is the Laplacian matrix associated with a directed graph containing a spanning tree, $x \in \mathcal{L}_p$ and $\widehat{x} \in \mathcal{L}_p$ if $y \in \mathcal{L}_p$ for $p \in [1, \infty]$ with $\widehat{x} = [x_1 - x_2, x_2 - x_3 ..., x_{n-1} - x_n]^T$ [36].

Lemma A-1. If $f, \dot{f} \in \mathcal{L}_\infty$ and $f \in \mathcal{L}_p$ for some $p = [1, \infty)$, then $f(t) \to 0$ as $t \to \infty$ [58].

The stability analysis should be decomposed into two steps:

Step 1: $\dot{V}_{d,o} \le 0$ from (50) implies that $V_{d,o}$, the orientation component of Lyapunov candidate V_d, defined in (46) is bounded and nonincreasing, which means $\varepsilon_{o,d} \in \mathcal{L}_\infty$, $\tilde{\theta}_{tr,o,i} \in \mathcal{L}_\infty$ and $\delta_o \in \mathcal{L}_2$. Considering that the desired trajectory x_{td} and its time derivative are bounded, then we have $\hat{\bar{o}}_{d,i} \in \mathcal{L}_\infty$ from (19) and further $\delta_o \in \mathcal{L}_\infty$ from (20). Together with the fact that $\gamma_o = [\gamma_{o,1}^T, ..., \gamma_{o,N}^T]^T \in \mathbb{R}^{3N}$ relates to δ_o by $\gamma_o = (\mathcal{L} + \mathcal{B})\, \delta_o$, $\gamma_o \in \mathcal{L}_\infty$ and further $\dot{\hat{\bar{o}}}_{d,i} \in \mathcal{L}_\infty$ with $\dot{\hat{\theta}}_{tr,o,i} \in \mathcal{L}_\infty$ can be obtained based on (23) and (24). Hence $\dot{\delta}_{o,i} \in \mathcal{L}_\infty$ from the derivative of (20). In addition, we have $\dot{\gamma}_{o,i} \in \mathcal{L}_\infty$ by differentiating (21), then $\ddot{\hat{\theta}}_{tr,o,i} \in \mathcal{L}_\infty$, $\ddot{\hat{\bar{o}}}_{d,i} \in \mathcal{L}_\infty$ and further $\ddot{\delta}_{o,i} \in \mathcal{L}_\infty$.

Conclusion 1: With the above analysis, $\delta_{o,i} \in \mathcal{L}_\infty \cap \mathcal{L}_2$, $\dot{\delta}_{o,i} \in \mathcal{L}_\infty$ and $\ddot{\delta}_{o,i} \in \mathcal{L}_\infty$ holds, then $\delta_{o,i} \to 0$ and $\dot{\delta}_{o,i} \to 0$ as $t \to \infty$ are achieved, $\forall i \in \{1, 2, ..., N\}$.

Step 2: Considering that $\delta_o = \hat{\bar{o}}_{d,i} - \bar{o}_{d,i}$, we have $\hat{\bar{o}}_{d,i} \to \bar{o}_{d,i}$ and $\dot{\hat{\bar{o}}}_{d,i} \to \dot{\bar{o}}_{d,i}$ as $t \to \infty$ based on the results of Conclusion 1. With the rigid transformation (18), $\hat{o}_{d,i} \to o_{d,i}$, $\dot{\hat{o}}_{d,i} \to \dot{o}_{d,i}$, $\hat{R}_{w,i} \to R_{w,i}$ and $\dot{\hat{R}}_{w,i} \to \dot{R}_{w,i}$ can be concluded since $R_{w,i}$ is the rotation matrix directly associated with the orientation of the desired local trajectory $o_{d,i}$. Therefore, $\tilde{\mathcal{T}}_{ji}, \dot{\tilde{\mathcal{T}}}_{ji}, \tilde{\mathcal{T}}_{ti}, \dot{\tilde{\mathcal{T}}}_{ti} \in \mathcal{L}_\infty$ and $\tilde{\mathcal{T}}_{ji}, \dot{\tilde{\mathcal{T}}}_{ji}, \tilde{\mathcal{T}}_{ti}, \dot{\tilde{\mathcal{T}}}_{ti} \to 0$ as $t \to \infty$ since $\widetilde{T}_{ji} = [((\hat{R}_{w,i} - R_{w,i})^i r_{ji})^T, 0_3^T]^T$ and $\widetilde{T}_{ti} = [((\hat{R}_{w,i} - R_{w,i})^i r_{ti})^T, 0_3^T]^T$. This further indicates that the variable $\bar{\rho}_i$ defined in (50) satisfies $\lim_{t \to \infty} \bar{\rho}_i = 0$ and $\bar{\rho}_i \in \mathcal{L}_\infty$. From (50), $\dot{V}_{d,p} = -\kappa \delta_p^T\, (\mathcal{Q} \otimes I_3)\, \delta_p / 2 \le 0$ when $\bar{\rho}_i = 0$, which means that closed-loop dynamics of position formation is input-to-state stable. Then following the similar proof procedure in Step 1, one can easily obtain that $\delta_{p,i} \to 0$ and $\dot{\delta}_{p,i} \to 0$ as $t \to \infty$ based on its input-to-state stability property with bounded vanishing disturbance. Together with Conclusion 1, the following conclusion can be stated:

Conclusion 2: The convergence of the trajectory estimation error is guaranteed, i.e., $\delta_i \to 0$ and $\dot{\delta}_i \to 0$ as $t \to \infty$, $\forall i \in \{1, 2, ..., N\}$. ∎

C. Proof of Theorem 2

Proof. Detail of (56) is presented in (A3). $\dot{V}_i \le 0$ implies that the Lyapunov candidate defined in (52) is always bounded and non-increasing, which immediately means $s_i \in \mathcal{L}_2 \cap \mathcal{L}_\infty$, $e_i \in \mathcal{L}_2 \cap \mathcal{L}_\infty$, $\dot{e}_i \in \mathcal{L}_2$, $\tilde{\theta}_{d,i}, \tilde{\theta}_{k,i}, \tilde{\theta}_{Id,i} \in \mathcal{L}_\infty$, $\tilde{x}_{o,i} \in \mathcal{L}_2 \cap \mathcal{L}_\infty$.

$$
\begin{aligned}
\dot{V}_i =& 2e_i^T \left(1-\frac{1}{K_\varepsilon}\right) K_{s,i}\Lambda_i \dot{e}_i - s_i^T \left(K_{\vartheta_i} - \frac{1}{2}\dot{\beta}_i J_{\phi,i}^T M_o J_{\phi,i}\right) s_i + \tilde{\theta}_{k,i}^T \Gamma_{k,i}^{-1} \dot{\tilde{\theta}}_{k,i} + \tilde{x}_{o,i}^T \alpha_i K_{o,i} \dot{\tilde{x}}_{o,i} \\
& - s_i^T \hat{J}_{e,i}^T K_{s,i} \hat{J}_{e,i} s_i + s_i^T J_{\phi,i}^T \tilde{F}_{I,i} - k_{r,i} (\hat{J}_{e,i} s_i)^T \hat{J}_{e,i} s_i \\
\leq & 2e_i^T \left(1-\frac{1}{K_\varepsilon}\right) K_{s,i}\Lambda_i \dot{e}_i + \tilde{\theta}_{k,i}^T \Gamma_{ki}^{-1} \dot{\tilde{\theta}}_{k,i} + \tilde{x}_{o,i}^T \alpha_i K_{o,i} \dot{\tilde{x}}_{o,i} - s_i^T \left(K_{\vartheta_i} - \vartheta_i\right) s_i + s_i^T J_{\phi,i}^T \tilde{F}_{I,i} \\
& - k_{r,i} \left\|\hat{J}_{e,i} s_i\right\|^2 - \left(S_{x,i} + Y_{k,i}\tilde{\theta}_{k,i} - \dot{\tilde{x}}_{o,i}\right)^T K_{s,i} \left(S_{x,i} + Y_{k,i}\tilde{\theta}_{k,i} - \dot{\tilde{x}}_{o,i}\right) \\
\leq & s_i^T J_{\phi,i}^T \tilde{F}_{I,i} - (S_{x,i} + \alpha_i \tilde{x}_{o,i})^T K_{s,i} (S_{x,i} + \alpha_i \tilde{x}_{o,i}) - s_i^T \left(K_{\vartheta_i} - \vartheta_i\right) s_i + \tilde{x}_{o,i}^T \alpha_i K_{o,i} \left(Y_{k,i}(\zeta_i, \dot{\zeta}_i)\tilde{\theta}_{k,i} - \alpha_i \tilde{x}_{o,i}\right) \\
& - k_{r,i} \left\|\hat{J}_{e,i} s_i\right\|^2 + \tilde{\theta}_{k,i}^T \Gamma_{k,i}^{-1} \dot{\tilde{\theta}}_{k,i} + 2e_i^T \left(1-\frac{1}{K_\varepsilon}\right) K_{s,i}\Lambda_i \dot{e}_i \\
\leq & -\alpha_i^2 \tilde{x}_{o,i}^T \left(K_{s,i} + K_{o,i}\right) \tilde{x}_{o,i} - 2\alpha_i K_{s,i} S_{x,i}^T \tilde{x}_{o,i} - s_i^T \left(K_{\vartheta_i} - \vartheta_i\right) s_i - S_{x,i}^T K_{s,i} S_{x,i} + s_i^T J_{\phi,i}^T \tilde{F}_{I,i} \\
& - k_{r,i} \left\|\hat{J}_{e,i} s_i\right\|^2 + 2e_i^T \left(1-\frac{1}{K_\varepsilon}\right) K_{s,i}\Lambda_i \dot{e}_i \\
\leq & -\left(1-\frac{1}{K_\varepsilon}\right) S_{x,i}^T K_{s,i} S_{x,i} + 2e_i^T \left(1-\frac{1}{K_\varepsilon}\right) K_{s,i}\Lambda_i \dot{e}_i - s_i^T \left(K_{\vartheta_i} - \vartheta_i\right) s_i - \alpha_i^2 \left(K_{s,i} + K_{o,i} - K_\varepsilon K_{s,i}\right) \tilde{x}_{o,i}^T \tilde{x}_{o,i} \\
& + s_i^T J_{\phi,i}^T \tilde{F}_{I,i} - k_{r,i} \left\|\hat{J}_{e,i} s_i\right\|^2
\end{aligned} \tag{A3}
$$

The collective form of (33) can be written as:

$$
\Delta x_o = -\left(\mathcal{E}\mathcal{L} \otimes I_6\right) \int_0^t \Delta x_o + e \tag{A4}
$$

where Δx_o and e are the column stack vectors of $\Delta x_{o,i}$ and e_i. $\mathcal{E} = \mathrm{diag}\left(\varepsilon_i\right)$ is a positive constant diagonal matrix. Then by using Corollary A-1, $\Delta x_{o,i}$, $\int_0^t \Delta x_{o,j} \in \mathcal{L}_2 \cap \mathcal{L}_\infty$, $\Delta x_{o,i} - \Delta x_{o,j} \in \mathcal{L}_2 \cap \mathcal{L}_\infty$, $\int_0^t \left(\Delta x_{o,i} - \Delta x_{o,j}\right) \in \mathcal{L}_2 \cap \mathcal{L}_\infty$ can be obtained from (A4) since $e_i \in \mathcal{L}_2 \cap \mathcal{L}_\infty$. This further yield $\int_0^t \Delta x_{o,i} \to 0$ and $\int_0^t \left(\Delta x_{o,i} - \Delta x_{o,j}\right) \to 0$ according to Lemma A-1. Since $\hat{\theta}_{k,i} \in \mathcal{L}_\infty$, $\hat{J}_{e,i}^\dagger(\zeta_i, \hat{\theta}_{k,i}) \in \mathcal{L}_\infty$ is guaranteed with the incorporated singularity-robust technique (36), $\dot{\zeta}_{r,i} \in \mathcal{L}_\infty$ can be concluded from (35) considering $e_i \in \mathcal{L}_\infty$ and boundedness of the estimated desired trajectories, i.e., $\hat{x}_{d,i}, \dot{\hat{x}}_{d,i} \in \mathcal{L}_\infty$. Then from (38), $s_i \in \mathcal{L}_\infty$ gives rise to $\dot{\zeta}_i \in \mathcal{L}_\infty$ and thus $\dot{x}_{e,i} = Y_{k,i}(\zeta_i, \dot{\zeta}_i)\theta_{k,i} \in \mathcal{L}_\infty$. In addition, $\dot{\tilde{x}}_{o,i} \in \mathcal{L}_\infty$ can be easily obtained from (32) and $\dot{\tilde{x}}_{o,i} = \dot{x}_{o,i} - \dot{x}_{e,i}$ further indicates $\dot{x}_{o,i}, \Delta\dot{x}_{o,i}, \Delta\dot{x}_{o,i} - \Delta\dot{x}_{o,j} \in \mathcal{L}_\infty$. Together with $\tilde{x}_{o,i} \in \mathcal{L}_2 \cap \mathcal{L}_\infty$, $\tilde{x}_{o,i} \to 0$ holds according to Lemma A-1. $\Delta x_{o,i} \to 0$, $\Delta x_{o,i} - \Delta x_{o,j} \to 0$ can be derived from Barbalat's lemma since $\int_0^t \Delta x_{o,i} \to 0$ and $\int_0^t \left(\Delta x_{o,i} - \Delta x_{o,j}\right) \to 0$. Based on the above analysis, $\Delta x_{e,i} \to 0$ and $\Delta x_{e,i} - \Delta x_{e,j} \to 0$ are guaranteed.

With $\dot{\zeta}_i \in \mathcal{L}_\infty$ and $\tilde{x}_{o,i} \in \mathcal{L}_\infty$, $\dot{\hat{\theta}}_{k,i} \in \mathcal{L}_\infty$ can be obtained from (43), which further gives rise to $\ddot{\zeta}_{r,i} \in \mathcal{L}_\infty$ considering that $\ddot{\hat{x}}_{d,i} \in \mathcal{L}_\infty$. Then from (41) and (29), the boundedness of the commanded torques is guaranteed, i.e., $\tau_i \in \mathcal{L}_\infty$.

The joint-space dynamics of the mobile manipulators (9) can be reformulated in its task space and the compact form of the constraint interconnected system's dynamics is given as:

$$
\bar{M}_x \ddot{\bar{X}} = \bar{F}_\Sigma + \bar{F}_E \tag{A5}
$$

where $\ddot{\bar{X}} = [\dot{v}_{\mathrm{obj}}^T, \dot{v}_{e,1}^T, ..., \ddot{v}_{e,N}^T]^T$ is the stack acceleration. $\bar{F}_E = [F_o^T, -F_{e,1}^T, ..., -F_{e,N}^T]^T$ is the stack interaction force. $\bar{M}_x = \mathrm{diag}(M_o, M_{x,1}, ..., M_{x,N})$ is the collective inertia matrix of the interconnected robotic system and $M_{x,i} = (J_{e,i}^T T_{A,i}^T)^\dagger M_{r,i} (T_{A,i} J_{e,i})^\dagger$ denotes the Cartesian-space counterpart of $M_{r,i}$. Let $F_{x,i} = (J_{e,i}^T T_{A,i}^T)^\dagger B_{r,i}\tau_i$ and $G_{x,i} = (J_{e,i}^T T_{A,i}^T)^\dagger G_{r,i}$ denote the Cartesian-space counterparts of the input joint torque τ_i and the gravity. $C_{x,i}\dot{x}_{e,i} = (J_{e,i}^T T_{A,i}^T)^\dagger C_{r,i}\dot{\zeta}_i - M_{x,i}(d(T_{A,i}J_{e,i})/dt)\dot{\zeta}_i$ is the Cartesian-space Coriolis/Centrifugal force. Then we have $\bar{F}_\Sigma = [(-C_o v_{\mathrm{obj}} - g_o)^T, \bar{F}_{x,1}^T, \bar{F}_{x,2}^T, ..., \bar{F}_{x,N}^T]^T$ in which $\bar{F}_{x,i} = F_{x,i} - C_{x,i}\dot{x}_{e,i} - G_{x,i}$.

Based on the analysis in [43], the closed-form of the interaction force $\bar{F}_E$ in our case here can be given as

$$
\bar{F}_E = A^T (A \bar{M}_x^{-1} A^T)^{-1} (b - A \bar{M}_x^{-1} \bar{F}_\Sigma) \tag{A6}
$$

where $b = [\left(S(\omega_1)^2 r_{o1}\right)^T, 0_3, ..., \left(S(\omega_N)^2 r_{oN}\right)^T, 0_3,]^T$ and $A = [-G_o^T, I_{6N}]$.

From (A6), one can conclude that $\bar{F}_E \in \mathcal{L}_\infty$ which further leads to $\ddot{\zeta}_i \in \mathcal{L}_\infty$, $\ddot{x}_{e,i} \in \mathcal{L}_\infty$ and $\dot{s}_i \in \mathcal{L}_\infty$ considering (9) and (38). Together with $\dot{\hat{\theta}}_{k,i} \in \mathcal{L}_\infty$, boundedness of $\dot{\hat{x}}_{e,i}$ can be guaranteed since $\dot{\hat{x}}_{e,i} = \dot{\hat{J}}_{e,i}(\zeta_i, \hat{\theta}_{k,i})\dot{\zeta}_i + \hat{J}_{e,i}(\zeta_i, \hat{\theta}_{k,i})\ddot{\zeta}_i$. Then from (30), $\ddot{x}_{o,i} \in \mathcal{L}_\infty$ can be concluded. This yields $\ddot{\tilde{x}}_{o,i} = \ddot{x}_{o,i} - \ddot{x}_{e,i} \in \mathcal{L}_\infty$, which means that $\dot{\tilde{x}}_{o,i}$ is uniformly continuous. Then according to Barbalat's Lemma, $\dot{\tilde{x}}_{o,i} \to 0$ is achieved since $\tilde{x}_{o,i} \to 0$ has been proved. Furthermore, since the estimated desired trajectory is also bounded, i.e., $\ddot{\hat{x}}_{d,i} \in \mathcal{L}_\infty$, then $\Delta\ddot{x}_{o,i} = \ddot{x}_{o,i} - \ddot{\hat{x}}_{d,i} \in \mathcal{L}_\infty$ and further $\Delta\ddot{x}_{o,i} - \Delta\ddot{x}_{o,j} \in \mathcal{L}_\infty$ can be guaranteed considering $\ddot{x}_{o,i} \in \mathcal{L}_\infty$. Together with $\Delta x_{o,i} \to 0$ and $\Delta x_{o,i} - \Delta x_{o,j} \to 0$, $\Delta\dot{x}_{o,i} \to 0$ and $\Delta\dot{x}_{o,i} - \Delta\dot{x}_{o,j} \to 0$ can be obtained. Similar to the preceding procedure, $\Delta\dot{x}_{e,i} \to 0$ and $\Delta\dot{x}_{e,i} - \Delta\dot{x}_{e,j} \to 0$ as $t \to \infty$, $\forall i \in \{1, 2, ..., N\}$.

Then we will give the analysis of internal force tracking error.

$$
\begin{aligned}
J_{\phi,i} M_{s,i}^{-1} J_{\phi,i}^T \tilde{F}_{I,i} =& J_{\phi,i} M_{s,i}^{-1} [(K_{\vartheta_i} + C_{s,i}) s_i - Y_{Id,i}\tilde{\theta}_{Id,i}] \\
& + J_{\phi,i}\dot{s}_i + J_{\phi,i} M_{s,i}^{-1} \hat{J}_{e,i}^T (K_{s,i} + k_{r,i}) \hat{J}_{e,i} s_i \\
& - J_{\phi,i} M_{s,i}^{-1} Y_{d,i}(\zeta_i, \dot{\zeta}_i, \dot{\zeta}_{r,i}, \ddot{\zeta}_{r,i}, \beta_i)\tilde{\theta}_{d,i}
\end{aligned} \tag{A7}
$$

with $s_i, \dot{s}_i \in \mathcal{L}_\infty$ and $\tilde{\theta}_{d,i}, \tilde{\theta}_{Id,i} \in \mathcal{L}_\infty$, the boundedness of $\tilde{F}_{I,i}$ is implied considering the positive definiteness of $J_{\phi,i} M_{s,i}^{-1} J_{\phi,i}^T$. ∎

REFERENCES

[1] M. Fruchard, P. Morin, and C. Samson, “A framework for the control of nonholonomic mobile manipulators,” *The International Journal of Robotics Research*, vol. 25, no. 8, pp. 745–780, 2006.

[2] G.-B. Dai and Y.-C. Liu, “Distributed coordination and cooperation control for networked mobile manipulators,” *IEEE Transactions on Industrial Electronics*, vol. 64, no. 6, pp. 5065–5074, 2017.

[3] S. Erhart and S. Hirche, “Adaptive force/velocity control for multi-robot cooperative manipulation under uncertain kinematic parameters,” in *2013 IEEE/RSJ International Conference on Intelligent Robots and Systems*. IEEE, 2013, pp. 307–314.

[4] P. Culbertson and M. Schwager, “Decentralized adaptive control for collaborative manipulation,” in *2018 IEEE International Conference on Robotics and Automation (ICRA)*. IEEE, 2018, pp. 278–285.

[5] A. Tsiamis, C. K. Verginis, C. P. Bechlioulis, and K. J. Kyriakopoulos, “Cooperative manipulation exploiting only implicit communication,” in *2015 IEEE/RSJ International Conference on Intelligent Robots and Systems (IROS)*. IEEE, 2015, pp. 864–869.

[6] J. Markdahl, Y. Karayiannidis, X. Hu, and D. Kragic, “Distributed cooperative object attitude manipulation,” in *2012 IEEE International Conference on Robotics and Automation*. IEEE, 2012, pp. 2960–2965.

[7] Y. Cao, W. Yu, W. Ren, and G. Chen, “An overview of recent progress in the study of distributed multi-agent coordination,” *IEEE Transactions on Industrial Informatics*, vol. 9, no. 1, pp. 427–438, 2013.

[8] Y. Ren, Z. Chen, Y. Liu, Y. Gu, M. Jin, and H. Liu, “Adaptive hybrid position/force control of dual-arm cooperative manipulators with uncertain dynamics and closed-chain kinematics,” *Journal of the Franklin Institute*, vol. 354, no. 17, pp. 7767–7793, 2017.

[9] F. Caccavale, P. Chiacchio, A. Marino, and L. Villani, “Six-dof impedance control of dual-arm cooperative manipulators,” *IEEE/ASME Transactions On Mechatronics*, vol. 13, no. 5, pp. 576–586, 2008.

[10] Y. Ren, Y. Liu, M. Jin, and H. Liu, “Biomimetic object impedance control for dual-arm cooperative 7-dof manipulators,” *Robotics and Autonomous Systems*, vol. 75, pp. 273–287, 2016.

[11] Z. Li, J. Li, and Y. Kang, “Adaptive robust coordinated control of multiple mobile manipulators interacting with rigid environments,” *Automatica*, vol. 46, no. 12, pp. 2028–2034, 2010.

[12] S. Erhart and S. Hirche, “Model and analysis of the interaction dynamics in cooperative manipulation tasks,” *IEEE Transactions on Robotics*, vol. 32, no. 3, pp. 672–683, 2016.

[13] Z. Yan, N. Jouandeau, and A. A. Cherif, “A survey and analysis of multi-robot coordination,” *International Journal of Advanced Robotic Systems*, vol. 10, no. 12, p. 399, 2013.

[14] Y. Kume, Y. Hirata, and K. Kosuge, “Coordinated motion control of multiple mobile manipulators handling a single object without using force/torque sensors,” in *2007 IEEE/RSJ International Conference on Intelligent Robots and Systems*. IEEE, 2007, pp. 4077–4082.

[15] H. Bai and J. T. Wen, “Cooperative load transport: A formation-control perspective,” *IEEE Transactions on Robotics*, vol. 26, no. 4, pp. 742–750, 2010.

[16] Z. Wang and M. Schwager, “Force-amplifying n-robot transport system (force-ants) for cooperative planar manipulation without communication,” *The International Journal of Robotics Research*, vol. 35, no. 13, pp. 1564–1586, 2016.

[17] G. Eoh, J. D. Jeon, J. S. Choi, and B. H. Lee, “Multi-robot cooperative formation for overweight object transportation,” in *2011 IEEE/SICE International Symposium on System Integration (SII)*. IEEE, 2011, pp. 726–731.

[18] J. Alonso-Mora, S. Baker, and D. Rus, “Multi-robot formation control and object transport in dynamic environments via constrained optimization,” *The International Journal of Robotics Research*, vol. 36, no. 9, pp. 1000–1021, 2017.

[19] Z. Peng, G. Wen, A. Rahmani, and Y. Yu, “Leader–follower formation control of nonholonomic mobile robots based on a bioinspired neurodynamic based approach,” *Robotics and Autonomous Systems*, vol. 61, no. 9, pp. 988–996, 2013.

[20] E. Montijano, E. Cristofalo, D. Zhou, M. Schwager, and C. Saguees, “Vision-based distributed formation control without an external positioning system,” *IEEE Transactions on Robotics*, vol. 32, no. 2, pp. 339–351, 2016.

[21] G. Antonelli, “Interconnected dynamic systems: An overview on distributed control,” *IEEE Control Systems*, vol. 33, no. 1, pp. 76–88, 2013.

[22] A. Marino, “Distributed adaptive control of networked cooperative mobile manipulators,” *IEEE Transactions on Control Systems Technology*, vol. 26, no. 5, pp. 1646–1660, 2017.

[23] G. Antonelli, F. Arrichiello, F. Caccavale, and A. Marino, “Decentralized time-varying formation control for multi-robot systems,” *The International Journal of Robotics Research*, vol. 33, no. 7, pp. 1029–1043, 2014.

[24] Z. Li, C. Yang, and Y. Tang, “Decentralized adaptive fuzzy control of coordinated multiple mobile manipulators interacting with non-rigid environments,” *IET Control Theory & Applications*, vol. 7, no. 3, pp. 397–410, 2013.

[25] C. K. Verginis, M. Mastellaro, and D. V. Dimarogonas, “Robust cooperative manipulation without force/torque measurements: Control design and experiments,” *IEEE Transactions on Control Systems Technology*, pp. 1–17, 2019, doi:10.1109/TCST.2018.2885682.

[26] A. Franchi, A. Petitti, and A. Rizzo, “Decentralized parameter estimation and observation for cooperative mobile manipulation of an unknown load using noisy measurements,” in *2015 IEEE International Conference on Robotics and Automation (ICRA)*. IEEE, 2015, pp. 5517–5522.

[27] A. Marino and F. Pierri, “A two stage approach for distributed cooperative manipulation of an unknown object without explicit communication and unknown number of robots,” *Robotics and Autonomous Systems*, vol. 103, pp. 122–133, 2018.

[28] A. Petitti, A. Franchi, D. Di Paola, and A. Rizzo, “Decentralized motion control for cooperative manipulation with a team of networked mobile manipulators,” in *2016 IEEE International Conference on Robotics and Automation (ICRA)*. IEEE, 2016, pp. 441–446.

[29] B. Siciliano, L. Sciavicco, L. Villani, and G. Oriolo, *Robotics: modelling, planning and control*. Springer Science & Business Media, 2010.

[30] T. Wimböck, C. Ott, A. Albu-Schäffer, and G. Hirzinger, “Comparison of object-level grasp controllers for dynamic dexterous manipulation,” *The International Journal of Robotics Research*, vol. 31, no. 1, pp. 3–23, 2012.

[31] F. Basile, F. Caccavale, P. Chiacchio, J. Coppola, and A. Marino, “A decentralized kinematic control architecture for collaborative and cooperative multi-arm systems,” *Mechatronics*, vol. 23, no. 8, pp. 1100–1112, 2013.

[32] S. Yu, B. Tao, Z. Gong, and J. Wang, “An efficient pose measurement method for end effector of mobile manipulator based on binocular stereovision,” in *2019 IEEE/ASME International Conference on Advanced Intelligent Mechatronics (AIM)*. IEEE, 2019, pp. 181–186.

[33] J. Peng, J. Yu, and J. Wang, “Robust adaptive tracking control for nonholonomic mobile manipulator with uncertainties,” *ISA Transactions*, vol. 53, no. 4, pp. 1035–1043, 2014.

[34] C.-C. Cheah, C. Liu, and J.-J. E. Slotine, “Adaptive jacobian tracking control of robots with uncertainties in kinematic, dynamic and actuator models,” *IEEE Transactions on Automatic Control*, vol. 51, no. 6, pp. 1024–1029, 2006.

[35] Y.-H. Liu and S. Arimoto, “Decentralized adaptive and nonadaptive position/force controllers for redundant manipulators in cooperations,” *The International Journal of Robotics Research*, vol. 17, no. 3, pp. 232–247, 1998.

[36] Z. Qu, *Cooperative control of dynamical systems: applications to autonomous vehicles*. Springer Science & Business Media, 2009.

[37] H. Yu and X. Xia, “Adaptive consensus of multi-agents in networks with jointly connected topologies,” *Automatica*, vol. 48, no. 8, pp. 1783–1790, 2012.

[38] J. Park and I. W. Sandberg, “Universal approximation using radial-basis-function networks,” *Neural Computation*, vol. 3, no. 2, pp. 246–257, 1991.

[39] A. Das and F. L. Lewis, “Distributed adaptive control for synchronization of unknown nonlinear networked systems,” *Automatica*, vol. 46, no. 12, pp. 2014–2021, 2010.

[40] P. Donner, S. Endo, and M. Buss, “Physically plausible wrench decomposition for multieffector object manipulation,” *IEEE Transactions on Robotics*, no. 99, pp. 1–15, 2018.

[41] I. D. Walker, R. A. Freeman, and S. I. Marcus, “Analysis of motion and internal loading of objects grasped by multiple cooperating manipulators,” *The International Journal of Robotics Research*, vol. 10, no. 4, pp. 396–409, 1991.

[42] S. Erhart and S. Hirche, “Internal force analysis and load distribution for cooperative multi-robot manipulation,” *IEEE Transactions on Robotics*, vol. 31, no. 5, pp. 1238–1243, 2015.

[43] D. Sieber and S. Hirche, “Human-guided multirobot cooperative manipulation,” *IEEE Transactions on Control Systems Technology*, 2018.

[44] A. Z. Bais, S. Erhart, L. Zaccarian, and S. Hirche, "Dynamic load distribution in cooperative manipulation tasks," in *2015 IEEE/RSJ International Conference on Intelligent Robots and Systems (IROS)*. IEEE, 2015, pp. 2380–2385.

[45] A. M. Schmidts, M. Schneider, M. Kühne, and A. Peer, "A new interaction force decomposition maximizing compensating forces under physical work constraints," in *2016 IEEE International Conference on Robotics and Automation (ICRA)*. IEEE, 2016, pp. 4922–4929.

[46] M. Namvar and F. Aghili, "Adaptive force-motion control of coordinated robots interacting with geometrically unknown environments," *IEEE Transactions on Robotics*, vol. 21, no. 4, pp. 678–694, 2005.

[47] K.-Y. Lian, C.-S. Chiu, and P. Liu, "Semi-decentralized adaptive fuzzy control for cooperative multirobot systems with h/sup/spl infin//motion/internal force tracking performance," *IEEE Transactions on Systems, Man, and Cybernetics, Part B (Cybernetics)*, vol. 32, no. 3, pp. 269–280, 2002.

[48] C. Liu, C. C. Cheah, and J.-J. E. Slotine, "Adaptive jacobian tracking control of rigid-link electrically driven robots based on visual task-space information," *Automatica*, vol. 42, no. 9, pp. 1491–1501, 2006.

[49] D. Sun and J. K. Mills, "Adaptive synchronized control for coordination of multirobot assembly tasks," *IEEE Transactions on Robotics and Automation*, vol. 18, no. 4, pp. 498–510, 2002.

[50] H. Wang, "Task-space synchronization of networked robotic systems with uncertain kinematics and dynamics," *IEEE Transactions on Automatic Control*, vol. 58, no. 12, pp. 3169–3174, 2013.

[51] ——, "Adaptive control of robot manipulators with uncertain kinematics and dynamics," *IEEE Transactions on Automatic Control*, vol. 62, no. 2, pp. 948–954, 2016.

[52] Y. Ren, Y. Zhou, Y. Liu, Y. Gu, M. Jin, and H. Liu, "Robust adaptive multi-task tracking control of redundant manipulators with dynamic and kinematic uncertainties and unknown disturbances," *Advanced Robotics*, vol. 31, no. 9, pp. 482–495, 2017.

[53] H. Chan and Ü. Özgüner, "Closed-loop control of systems over a communications network with queues," *International Journal of control*, vol. 62, no. 3, pp. 493–510, 1995.

[54] Y.-H. Wei, Q. Leng, S. Han, A. K. Mok, W. Zhang, and M. Tomizuka, "Rt-wifi: Real-time high-speed communication protocol for wireless cyber-physical control applications," in *2013 IEEE 34th Real-Time Systems Symposium*. IEEE, 2013, pp. 140–149.

[55] FRANKA EMIKA. (2017) "franka control interface documentation". (Assessed on July 1, 2019). [Online]. Available: https://frankaemika.github.io/docs/

[56] S. Haddadin, A. De Luca, and A. Albu-Schäffer, "Robot collisions: A survey on detection, isolation, and identification," *IEEE Transactions on Robotics*, vol. 33, no. 6, pp. 1292–1312, 2017.

[57] W. Li and M. W. Spong, "Stability of general coupled inertial agents," *IEEE Transactions on Automatic Control*, vol. 55, no. 6, pp. 1411–1416, 2010.

[58] P. A. Ioannou and J. Sun, *Robust adaptive control*. PTR Prentice-Hall Upper Saddle River, NJ, 1996, vol. 1.

Yi Ren received the bachelor degree in Thermal Energy and Power Engineering from Harbin Institute of Technology, Harbin, China in 2011. Then he received the M.Sc. degree and Ph.D degree in Mechatronic Engineering all from Harbin Institute of Technology, Harbin, China, in 2013 and 2017. Since 2018, he has been working as a postdoc in Electrical Engineering at Chair of Information-oriented Control, Department of Electrical and Computer Engineering, Technical University of Munich, Munich, Germany. His research interests include robotics, nonlinear control, vision-based control and distributed control with application to multi-robot cooperation and manipulation.

Stefan Sosnowski received the Dipl.-Ing. degree and Dr.-Ing. degree in electrical engineering from the Technical University of Munich (TUM), Munich, Germany, in 2007 and 2014, respectively. He is a Postdoctoral Fellow with the Chair of Information-oriented Control, TUM, since 2014. He has authored and coauthored more than 30 journal papers, conference proceedings, and book chapters on bioinspired robotics.

Dr. Sosnowski received awards such as the Best Paper Award of the International Federation of Automatic Control World Congress of Maneuvering and Control of Marine Craft in 2009, Finalist Best Paper Award of the International Conference on Social Robotics in 2010, the most innovative video award of the AI Video Competition of the International Joint Conferences on Artificial Intelligence in 2009, and Finalist Best Video Award of the International Conference on Robotics and Automation in 2008 as well as the Frontier Science Conference Series admission for outstanding young Japanese or European researchers from the European Science Foundation (ESF) and Japan Society for the Promotion of Science (JSPS) in Kanagawa, Japan

Sandra Hirche (M'03-SM'11-F'20) received the Diplom-Ingenieur degree in aeronautical and space engineering from Technical University Berlin, Berlin, Germany, in 2002 and the Doktor-Ingenieur degree in electrical engineering from the Technical University of Munich (TUM), Munich, Germany, in 2005.

From 2005 to 2007, she received the Postdoc scholarship from the Japanese Society for the Promotion of Science, Fujita Laboratory, Tokyo Institute of Technology, Tokyo, Japan. From 2008 to 2012, she was an Associate Professor with the Technical University of Munich. Since 2013, she has been the TUM Liesel Beckmann Distinguished Professor and the Chair of Information-oriented Control with the Department of Electrical and Computer Engineering, TUM. She has published more than 200 papers in international journals, books, and refereed conferences. She has received multiple awards such as the Rohde & Schwarz PhD Award, the Best Poster Award of the 2005 International Federation of Automatic Control World Congress, the Best Paper Award of the 2009 IEEE World Haptics, and the Outstanding Student Paper Award of the 2018 IEEE Conference on Decision and Control. In 2013 she has been awarded with a Starting Grant on the "Control based on Human Models" and in 2019 with a Consolidator Grant on "Safe data-driven control for human-centric systems" by the European Research Council (ERC). Her main research interests include learning, cooperative, distributed, and networked control with applications in human-robot interaction, multi-robot systems, and general robotics.